A REVIEW OF SOME RECENT DEVELOPMENTS IN HYPERSONIC FLOW*

By Antonio Ferri

Polytechnic Institute of Brooklyn

INTRODUCTION†

The field of hypersonic aerodynamics is dominated by two conflicting characteristics: The phenomena to be investigated are much more complex and less amenable to simplified schemes of analysis and to experimental investigation than other fields of fluid dynamics while at the same time much more precise detailed knowledge of the flow field is required in order to obtain the information necessary for practical applications.

The complexity of hypersonic flow can be attributed to two main reasons: In very high speed flow fields of practical interest the fluid behaves as nonideal gas with variable properties; chemical-physical transformations can take place in limited regions of the flow; at the same time the flow to be investigated is highly nonlinear, rotational and, in important regions, of the transonic type.

Against this formidable increase of difficulties with respect to supersonic flow stands the necessity of obtaining more accurate and more detailed information of the flow field. In hypersonic flow problems, it is important to determine the heat transfer to the body together with the determination of forces and pressure distribution. For the determination of the forces only integral characteristics of the flow field are required; these can be obtained by means of simplified representations of the overall phenomenon, without the necessity of representing correctly the details of the flow, while the determination of heat transfer requires a precise knowledge of velocity and pressure gradients, of pressure and entropy distributions in the flow field, of chemical-physical transformations taking place inside and outside the boundary layer, and of laminar, turbulent and transitional boundary layer flows. In spite of all these difficulties very rapid progress has been obtained in this field in the last few years, due to the continuous interest of large scientific groups and of military organizations.

* This work was supported by the United States Air Force through the Office of Scientific Research, Air Research and Development Command, under Contract AF 49(638)-217, and through the Aeronautical Research Laboratory of Wright Air Development Center, under Contract No. 33(616)-3265.

† For list of symbols used in this paper, see end of text.

It is the scope of this paper to review briefly a few of the more recent contributions obtained in this field and to discuss some of the problems that require more consideration in the future. The new results presented in this paper have been obtained with the co-operation of the staff of the Aerodynamics Laboratory of the Polytechnic Institute of Brooklyn. I should like to mention specifically Dr. Roberto Vaglio-Laurin for his help in connection with the analytical work related to the pressure distribution, Mr. Victor Zakkay in connection with the experimental work, and Dr. Paul A. Libby for his contributions and suggestions in the preparation of this report.

1. CHEMICAL-PHYSICAL EFFECTS

In order to discuss the effects of chemical-physical transformations taking place in the fluid on aerodynamic characteristics, hypersonic flow fields can be grouped in two major categories: The fields where the flows can be considered everywhere to be in thermodynamic equilibrium, and the fields where nonequilibrium conditions exist and produce noticeable first order aerodynamic effects.

In many of the hypersonic flow fields of practical interest a large static temperature rise occurs in localized regions of the flows. Because of the large absolute value of the stagnation enthalpy, large variations of gas properties take place in these regions. In the lower range of Mach number the internal energy of the gas is essentially entirely represented by the translational and rotational energy of the molecules, and the energy and state equations can be represented by:

$$E = (\beta - 1)\frac{p}{\rho} = \frac{1}{\gamma - 1}\frac{p}{\rho} \text{ and}$$

$$\frac{p}{\rho} = RT \tag{1.0}$$

where R and γ are constant. At higher static temperatures also vibration, dissociation, and ionization energy contribute to the energy content of the gas. Then the expression for internal energy must be modified and the quantity β must be considered as a summation of different contributions and the equation of state must have a corrective term

$$\frac{p}{\rho} = RZT \tag{1.1}$$

which takes into account the effects of dissociation and ionization.

When the variations of the physical properties of the gas due to the aerodynamic phenomena take place gradually, and the times corresponding to significant variations of physical properties are large with respect to the relaxation times of the different degrees of freedom of the particles,

it can be assumed with sufficient approximation that the flow is at each point in statistical equilibrium. In this case the properties of the gas (as β and Z) are functions only of local conditions (pressure and temperature). However, the mechanism for reaching equilibrium depends on the kinetics and probability of collisions. Therefore, the relaxation time for equilibrium depends on pressure and temperature. For high altitude and high velocity flight the mean free path for equilibrium of vibration, dissociation and ionization, becomes large and in many cases can no longer be considered small with respect to a typical dimension of the flow field where large accelerations or decelerations occur. Then the simplifying assumption of equilibrium conditions is not valid.

A large amount of work has been done in the field of equilibrium flow problems. A detailed analysis of the properties of air for equilibrium conditions as a function of pressure and temperature has been performed by several groups[1–6]. Mollier charts for air are available[7,8] and polynomials or charts representing conveniently the properties of air in a given range of pressure and temperature have been developed[9]. By means of these data, it is possible in principle to extend the numerical methods of analysis developed for constant gas properties to the case of variable properties without any conceptual additional complication. The numerical work becomes more complex and must be carried out for various altitudes. The introduction of large scale computing machines tends to overcome this complication. Moreover, the variation of gas properties tends to complicate any type of analytical method, which by necessity requires the introduction of simplifying assumptions.

Tables giving the changes of flow properties across shocks are also readily available, and simple one-dimensional type problems such as conical flows have also been determined for real gas equilibrium condition. Some of the available data are given[7, 10, 11, 12].

The variation of gas properties in the flow field tends to complicate also the experimental techniques because of the necessity of simulating in the test the variation of flow properties with pressure and temperature. This variation can be simulated if stagnation temperatures and stagnation pressure are exactly represented, and thermodynamic equilibrium exists. At present simulation of Mach number, Reynolds number and stagnation conditions is very difficult to obtain. However, it is standard procedure in experimental aerodynamics because of the difficulty of complete representation, to study separately the effects of different parameters in order to introduce corrections to experimental data more readily obtainable. This approach can be used probably to correct measurements of forces and pressure distributions determined at the correct Mach numbers but without the simulation of real gas effects.

Experimental and analytical evidence tends to indicate that the real gas effects on the pressure distribution on the front part of blunt bodies (where the static temperature is high) are not too important, while in the

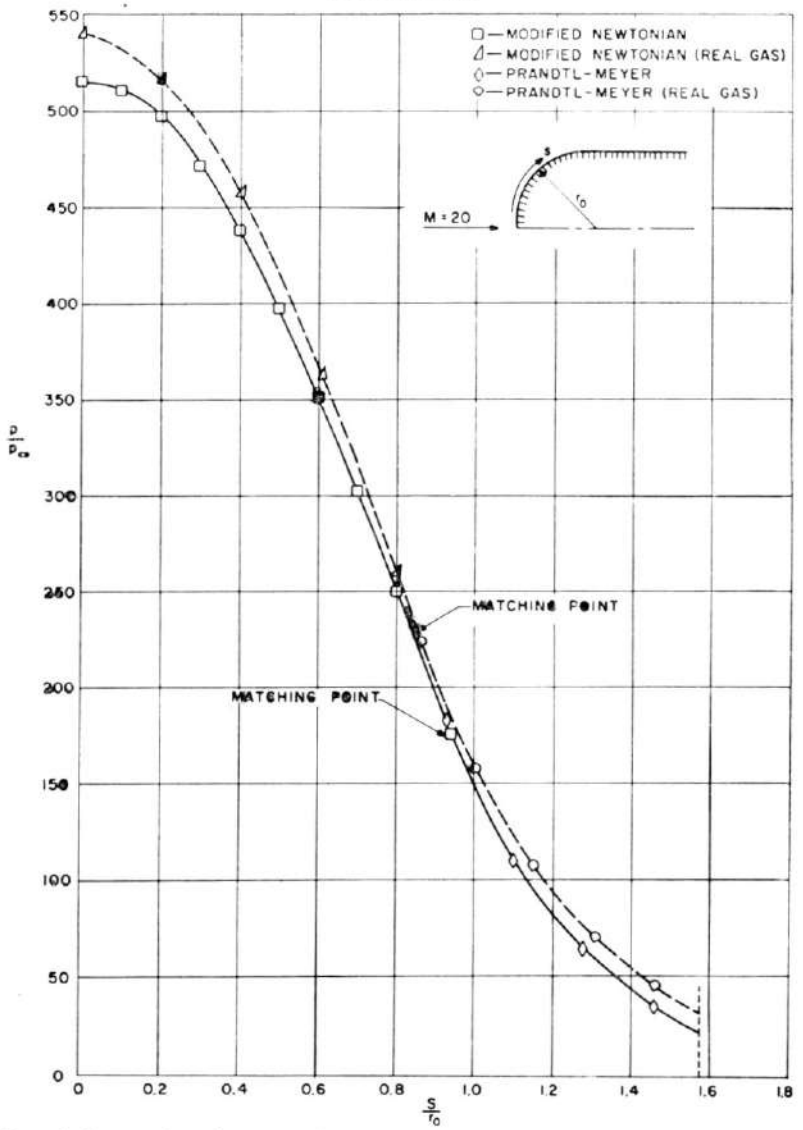

FIG. 1. Comparison between theoretical ideal and real gas pressure distribution along a hemisphere cylinder body at $M=20$ at 100,000 ft altitude.

high local Mach numbers region, because of the low static temperature, the gas is not far from an ideal gas. For example, a comparison between values of pressure distribution along a hemisphere cylinder at $M=20$ for ideal gas and real gas is presented in Fig. 1. The values have been obtained by modified Newtonian followed by Prandtl–Meyer expansion. The matching point has been chosen at the point of tangency of the two laws. It has been shown that this type of analysis gives good approximation in hypersonic flow. The effects of real gas on the ratio p/p_∞ are small, and the effects on

the ratio p/p_s are even smaller. Here p is the local static pressure on the surface, p_s is the stagnation pressure behind a normal shock and p_∞ is the undisturbed static pressure.

At present, both numerical analysis for a limited range of simple boundary conditions or experimental investigations without full stagnation simulation can give sufficient data which permit taking into account approximately real gas effects as far as pressure distribution and force determination are concerned.

The field of nonequilibrium aerodynamics is in a much less advanced stage. Few theoretical and experimental results are available at present; these are essentially aimed at defining the conditions under which nonequilibrium phenomena affect the flow field properties sizeably[13–17]. Few theoretical attempts to determine analytically the mean free path for vibration and dissociations are available[13–15,17]. All these methods try to obtain the order of magnitude of the mean free path from collision kinetics and collision probabilities. Because of the relatively poor knowledge of the many parameters involved, the analyses in question are somewhat of a qualitative nature, and do not give sufficiently accurate physical information as is required for an investigation of the related effects on the flow field.

A great amount of work has been performed in order to determine experimentally vibration and dissociation relaxation times. Some of the more recent results are presented in refs. 15, 17, 18, 19, 20, 21, 22. In ref. 17 preliminary data indicating the region of validity of the assumption of aerodynamic equilibrium are presented. These data tend to indicate that nonequilibrium conditions in the inviscid flow region can be important above altitudes on the order of 200,000 ft for flight speeds about $M=20$.

Non-equilibrium effects could be important for the flow inside the boundary layer in a range of altitude and Mach number much below the aforementioned values, because here the physical dimension to be compared with the relaxation mean free path is the boundary layer thickness. In the boundary layer the finite relaxation lengths for vibration, dissociation and ionization, and the possibility of diffusion of atoms and ions, which can subsequently recombine, may add appreciably to the value of heat transfer produced by molecular conduction.

The analysis of real gas and nonequilibrium effects on the flow inside the boundary layer effects has been conducted along two different lines. In ref. 23 detailed investigations of these effects for the laminar heat transfer at the stagnation point of blunt bodies has been performed, and the contribution of nonequilibrium real gas effects has been obtained. In ref. 24 two limiting cases have been investigated; the first assumes thermodynamic equilibrium, the second assumes very slow recombination rates, and diffusion as the governing phenomenon in the flow. In both cases small effects due to real gas properties have been found. These

effects are of the same order as the effects produced by small aerodynamic changes in the flow field, and can be considered small when the uncertainty of experimental measurements, and of the theory of laminar, transitional and turbulent boundary layer is taken into account.

Experimental results obtained in shock tubes[25] indicate good agreement with the analysis for real gas in equilibrium[23] or with an analysis that neglects dissociation. These data are presented in Fig. 2.

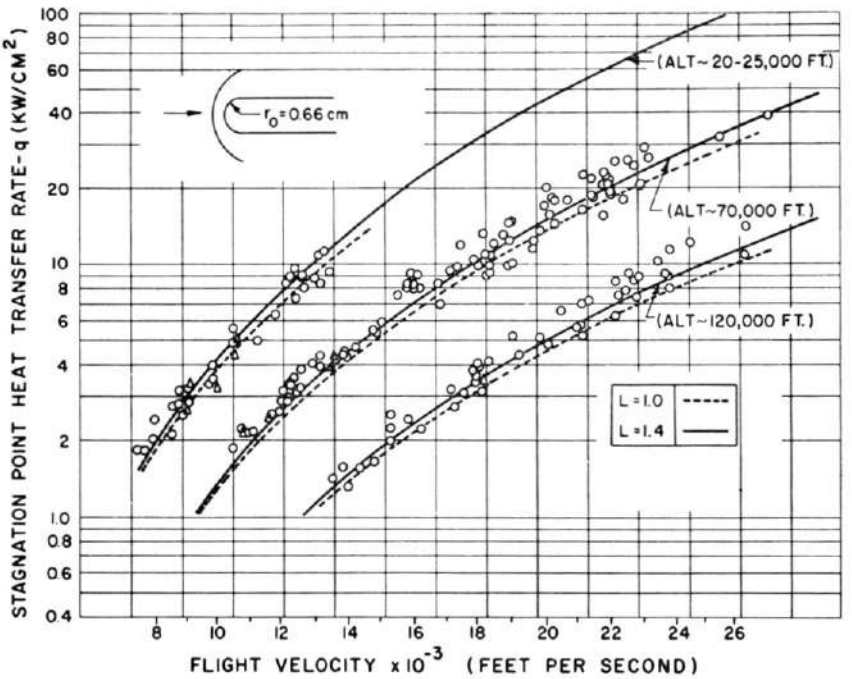

FIG. 2. Comparison between experimental ideal and real gas heat transfer at the stagnation point of a blunt body ($L=1$ ideal gas, $L=1{\cdot}4$ real gas)[25].

The effects of real gas and equilibrium conditions are represented by the difference between dotted and solid lines. This figure could give the misleading impression that the value of heat transfer coefficient can be determined only if correct stagnation pressure and temperature are simulated. This, however, appears not to be the case. The stagnation point heat transfer given in ref. 23 is expressed as

$$q_s = 0{\cdot}76\, Pr^{-0{\cdot}6} \left(\frac{\rho_w \mu_w}{\rho_{s_e} \mu_{s_e}}\right)^{0.1} (h_{s_e} - h_w) \sqrt{\rho_{s_e} \mu_{s_e} \left(\frac{du_e}{ds}\right)} \times$$

$$\left[1 + (L^{0{\cdot}52} - 1)\, \frac{h_D}{h_{s_e}}\right] \tag{1.2}$$

where the subscript w represents wall conditions and s_e external stagnation conditions; h is the enthalpy and Pr the Prandtl number. From Eq. (1.2) the coefficient $Nu/Re^{\frac{1}{2}}$ can be determined, where the Nusselt number Nu and the Reynolds number Re are referred to external properties and to a typical dimension of the body. The pressure and velocity near the stagnation point can be expressed as dimensional parameters in the form:

$$\frac{p}{p_s} = 1 - K\bar{s}^2 \tag{1.3}$$

and

$$\bar{u} = u_e/\sqrt{h_{s_e}} \tag{1.4}$$

where $\bar{s}=s/r_0$ and r_0 is a dimension defining the geometry of the nose, for example, the radius of the curvature at the stagnation point. The Nusselt and Reynolds numbers can be expressed as[82]

$$Nu = q_w (c_p)_{s_e} r_0/k_{s_e}(h_{s_e} - h_w); \tag{1.5}$$

$$\overline{Re} = Re\sqrt{p_s/\rho_{s_e} h_{s_e}};\ Re = \rho_{s_e}\sqrt{h_{s_e}}\, r_0/\mu_{s_e} \tag{1.6}$$

then

$$\frac{Nu}{\overline{R}^{\frac{1}{2}}} = 0{\cdot}794\sqrt{K}\left(\frac{\rho_w \mu_w}{\rho_{s_e}\mu_{s_e}}\right)^{0{\cdot}1}\left[1 + (L^{0{\cdot}52} - 1)\frac{h_D}{h_{s_e}}\right] \tag{1.7}$$

where the Prandtl number has been assumed equal to 0·71. Because of the low value of the exponential of the term $\rho_w \mu_w/\rho_{s_e}\mu_{s_e}$ it appears that large variations of the ratio h_w/h_{s_e} can occur without affecting the value of

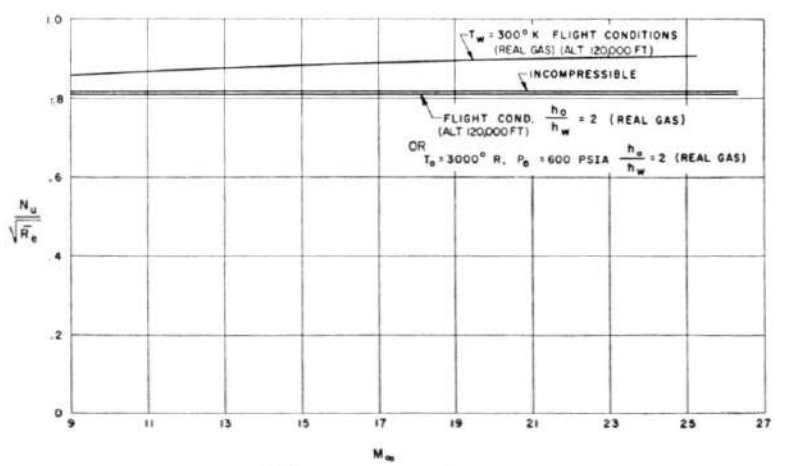

FIG. 3. Variation of $Nu/\sqrt{\overline{Re}}$ at the stagnation point as a function of flight. Mach number M_∞ for real and ideal gas and different stagnation and wall conditions (t_0, h_0, p_0 stagnation temperature, enthalpy and pressure, t_w, h_w wall temperature and enthalpy).

$Nu/\bar{R}^{\frac{1}{2}}$ significantly. The effect of dissociation and diffusion is represented by the second term of the expression inside the brackets. If $L=1$ this term is zero. In ref. 23 the value of 1·4 has been assumed for L. In Fig. 3 the values of $Nu/\bar{R}e^{\frac{1}{2}}$ obtained from Eq. (1.7) are presented as a function of flight Mach number for different values of h_{s_e}/h_w, the ratio of stagnation enthalpy to wall enthalpy, and two stagnation wind tunnel conditions. As shown in Fig. 3 the value of $Nu/\bar{R}e^{\frac{1}{2}}$ is very slightly affected by all these parameters, indicating that results of experiments where real gas effects are not simulated would still give good practical information. For comparison the values obtained from the incompressible flow analysis of ref. 26 are also shown. It could be expected that these parameters may be important downstream of the stagnation point. However, the results of simple analysis tend to show that this is not the case.

In Fig. 4 a comparison is made between the heat transfer along a sphere

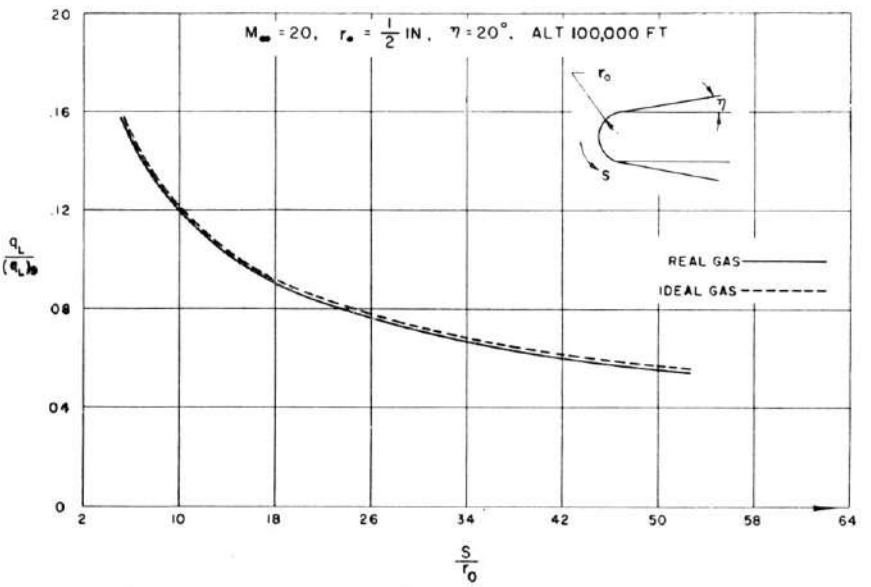

FIG. 4. Comparison between equilibrium real and ideal gas heat transfer distribution along a blunt 20° cone at $M_\infty = 20$ and 100,000 ft altitude (q_L = local heat transfer coefficient, $(q_L)_0$ = stagnation heat transfer coefficient).

cone obtained by assuming that the gas is a real gas or a perfect gas both in equilibrium. In the figure the ratio q_L/q_{L_0} between the local and the stagnation point heat transfer along the length of the body is presented. The analysis has been performed according to the method presented in ref. 24. The difference between the two curves is negligible*. As for the

* Rep. No. 15 of AVCO Res. Lab. by N. H. Kemp, P. H. Rose and R. W. Detra, "Laminar Heat Transfer Around Blunt Bodies in Dissociated Air", has become available after the preparation of this report. The results presented there confirm these conclusions.

region of inviscid flow the effects of real gas on boundary layer phenomena at very low density or Reynolds number are yet unknown. It can be expected that for these conditions these effects can be large.

2. DETERMINATION OF THE PRESSURE DISTRIBUTION

(a) *Two-dimensional or Axially Symmetric Flow Fields*

The problem of determination of pressure distribution for two-dimensional or axially symmetric hypersonic flow fields when the flow is of hyperbolic type does not present any additional conceptual complication over the determination of supersonic rotational flows even when variable gas properties must be considered. As for the case of supersonic rotational flows, when two family waves must be considered, numerical methods are usually required. In the case of variable gas properties, additional equations that represent the variation of gas properties with pressure and temperature must be added. A practical approach that is convenient when automatic computing machines are used is to express the gas properties by means of polynomials. Polynomials of this type have been suggested by the Army Ballistic Missile Agency

$$\frac{S}{R} = \sum_{i=0}^{4} \sum_{j=0}^{5} A_{ij} (P)^i (h)^j \tag{2.1}$$

$$\frac{S}{R} = \sum_{m=0}^{4} \sum_{n=0}^{5} B_{mn} Q^m h^n \tag{2.2}$$

where

$$P = \log \frac{p}{p_{\text{atm}}} \qquad Q = \log \frac{\rho}{\rho_{\text{atm}}} \tag{2.3}$$

S is the entropy and R is the gas constant. The coefficients A_{ij}, B_{mn} have been determined from the Mollier diagram. The characteristic equations can be written as

$$\frac{\mathrm{d}p}{\gamma' p} \sin \mu \cos \mu \pm \mathrm{d}\theta + \frac{\sin \mu \sin \theta}{\cos(\theta \pm \mu)} \frac{\mathrm{d}x}{y} = 0 \tag{2.4}$$

where

$$\gamma' = \frac{\rho}{p} \left(\frac{\partial p}{\partial \rho} \right)_s \tag{2.5}$$

and can be obtained directly from the expression (2.1) and (2.2).

Some complication can arise because of the fact that the growth of the boundary layer could require some correction in the boundary conditions used for the inviscid flow field. However, in practical cases for low altitudes these corrections are usually small, and if required can be obtained in first

approximation from a preliminary analysis of the boundary layer growth on the basis of rough estimate of pressure distributors.

The special problem discussed in refs. 28–33 existing at the sharp leading edge of a two-dimensional plate is a very interesting academic problem, but with small practical significance. For sharp edges, small changes in the physical thickness of the edge can produce effects of the same order of those produced by the boundary layer growth; this behavior is due to the presence of the highly curved shock along the leading edge, generated by the physical thickness of the edge. The large entropy gradient induces very large pressure gradient that extends for a length, that is, of an order of magnitude larger than the thickness of the edges[34]; therefore, a precise knowledge of the geometry of the edge is required. At very low density this problem of interference will become important for many types of boundary conditions.

In many practical applications, the front part of the body is blunt in order to reduce the local heat transfer; therefore, the problem of analysis of blunt bodies at hypersonic speed has lately received large attention. At present the majority of the experimental or theoretical work has been concentrated on the analysis of axially symmetric or two-dimensional flow over blunt bodies. Approximate analytical methods have been developed and several numerical methods are also presently available. A critical review of some of the analytical methods has been presented in ref. 34, and some of the original reports dealing with this problem are given in refs. 35 to 61. Of all the approximate analytical methods, the methods suggested in ref. 47 and reconsidered in ref. 48, and called the modified Newtonian approximation, is the simplest. It gives a good approximation for bodies having small changes of the curvatures between the stagnation point and the sonic line. Good results have also been obtained by assuming incompressible rotational flow near the stagnation point and simplifying assumptions in the other part of the flow field[35]. This direction is of interest because it could give information also for bodies without axial symmetry.

Several directions have been taken in order to improve the Newtonian approximations[52,53]. Difficulties have been found in these approaches due to the poor convergency of the series used. A detailed discussion of this problem is presented in ref. 34. Recently, numerical methods have been developed for the analysis of the flow field in the elliptic and transonic regions[55–61]. All the methods consider the inverse problem where the shock shape is given and the body shape must be determined. The numerical solution of the direct problem where the body shape is given and the shock must be determined, presents serious difficulties because it requires the determination of the entropy distribution in the flow field without a detailed knowledge of the shock shape. Of these methods the method discussed in refs. 55–56 transforms the elliptic type problem of the analysis of the subsonic flows in a hyperbolic type problem by intro-

ducing a fictitious third dimension that is similar to a time variable. In this approach the problem of instability, characteristic of the initial value problems of elliptic type, is eliminated; therefore, from this point of view, the method is mathematically more satisfactory than others. However, the amount of numerical work is notably increased. A different type of solution is required in order to pass from the subsonic to supersonic region.

All the methods listed use finite difference approximations. The problem of computational instability in some cases is investigated numerically by perturbation of the initial data. All the results published until now, assume completely analytic shapes for the shock and therefore theoretically lead to the determination of the flow field in the subsonic and transonic region without the necessity of special consideration of the shape of the sonic line. However, in ref. 60 a special consideration is given to the determination of the sonic line.

For flat-nosed bodies the shape of the body near the region of the sonic line has a marked influence in all the flow fields and the shape of the sonic line is more strongly influenced by the body shape than the shock shape. Therefore, in this case it can be convenient to assume as boundary conditions the shock shape in the elliptic region and the shape of the sonic line. From conditions of mass continuity and from the shock shape the direction of velocity along the sonic line can be determined, and then the flow in the elliptic region can be obtained by finite difference methods. This possibility has been a leading consideration in the approach presented in ref. 60. This approach is particularly useful when bodies with corners or large curvature at the sonic line are considered. At a corner of the body a singularity exists. The type of singularity can be obtained from ref. 62 because the entropy gradient normal to the streamline does not affect the singularity.

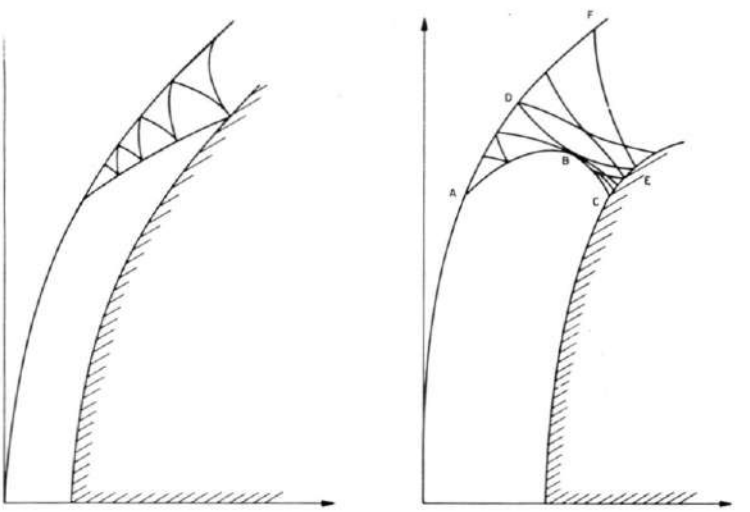

FIG. 5. Schematic representation of the flow field near the sonic line for blunt bodies.

The shape of the sonic line corresponding to a given body shape at the shoulder and to a given shock shape can be assumed in first approximations by knowing the inclination and curvature of the sonic line at the shock from mass flow considerations and from the curvature of the sonic line at the corner. The curvature of the sonic line at the body can be obtained from the curvature of the body and from the entropy gradient.

In Fig. 5 there are given schematically the shapes of shock, sonic line and characteristic net in the transonic region for two bodies, one having gradual curvature and the other having a more rapid curvature near the sonic line. In the first case, the sonic line is determined directly from the shock and the characteristic lines reaching the sonic line all start from the shock. In the second case, some of the characteristic lines start from the body, then the flow at the sonic line between points B and C is influenced by the body shape. This part of the flow field is defined if the shock is given between the axis and point F. However, it can be seen that localized changes in the shock in the region between the point D and point F will influence the shape of the sonic line, the shape of the body, and thus all the flow in

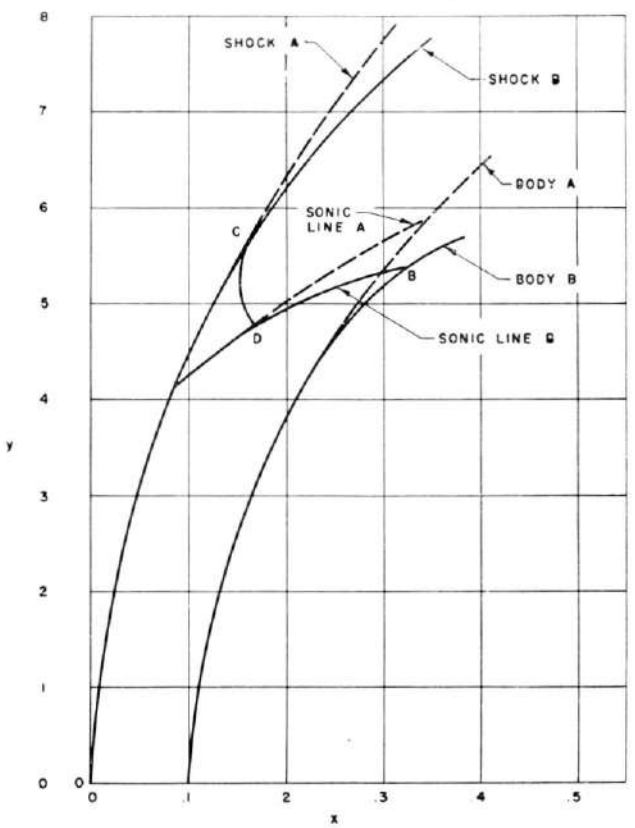

FIG. 6. Shape of bodies corresponding to slightly different boundary conditions at the sonic line for $M_{00} = 20$.

the elliptic region. Therefore, any analysis of the elliptic region starting only from the shock needs to consider carefully the values of very high order derivatives of the flow properties at the shock. This consideration indicates that numerical procedures starting only from an analytical shock in the elliptic region can be insensitive to small changes of body shape. This difficulty can be eliminated by assuming as boundary conditions for the elliptic region, the shape of the shock in the elliptic region and the shape of the sonic line or by extending the numerical calculations well inside the supersonic region. In this respect the approach, wherein the sonic line is determined or assumed and then is considered as part of the boundary conditions for the elliptic region, is less open to criticism.

In order to clarify this point, it may be of interest to show results of a calculation performed for two different boundary conditions. The shock shape in the elliptic region is similar for the two calculations in the sense that the equation representing the two shocks gives the same co-ordinates and the same derivatives to the order considered in the analysis at all the points carried in the numerical calculations. Also the shocks in the supersonic region are similar up to the point C; within the approximation of the analysis, the sonic lines are then equal up to point D (Fig. 6). In one case the complete shock shape, given by the expression

$$x = Ky^2$$

is chosen as a boundary condition (Body A). The shape of the sonic line is obtained from the shock (ref. 60). In the second case, the same shock shape in the region OC and for the remaining part of the flow, the shape of the sonic line DB has been chosen as boundary conditions. The entropy and the flow direction at the sonic line can be obtained from energy, momentum and mass continuity considerations. The shapes of the two bodies are shown in Fig. 6. The difference of the body shape at the shoulder is appreciable. In Fig. 7 the pressure distributions on the two bodies are indicated*.

When the transonic region is determined, then the flow field in the hyperbolic region can be obtained by means of the method of characteristics. However, this method is lengthy; therefore other simpler approximate analyses have been suggested[63–71]. Both Prandtl–Meyer expansion and blast wave theory have been used recently with apparent agreement with experimental data. The Prandtl–Meyer expansion neglects the effect of the second family waves. This effect, produced by the entropy gradients, can be in some cases very large. As an example, this analysis would not be able to predict the decay of pressure which occurs along a flat slab following a wedge[33] (Fig. 8) which in this case is very large. The entropy effects are considered in the blast wave theory of refs. 63, 64, 65, 66, 71. Therefore, it can be expected that the blast wave theory can predict more

* This work has been performed with the co-operation of Dr. Roberto Vaglio-Laurin.

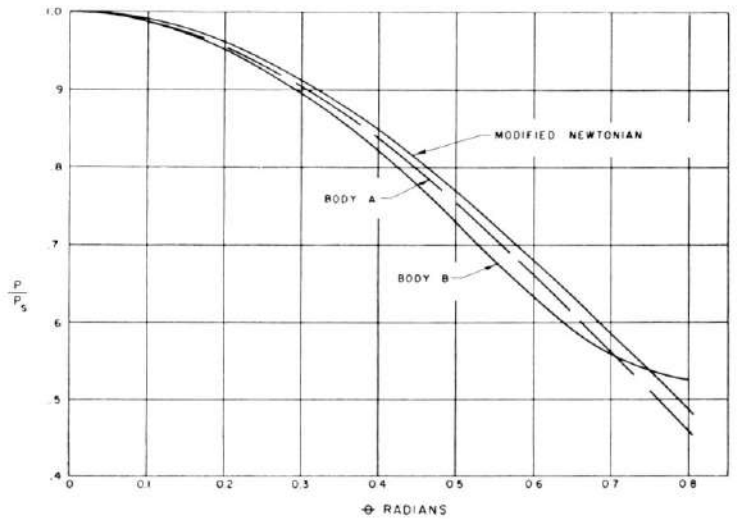

FIG. 7. Calculated pressure distribution as a function of the local inclination θ for two blunt bodies having variation of the shock shape only in the supersonic region of the flow for $M_{00} = 20$.

accurately the shape of the pressure distribution and the rate of pressure decay. This theory presents the difficulty of the uncertainty of the origin of the co-ordinates, and therefore can be used only downstream from the nose but within the region of influence of the strong part of the shock wave. In order to orient the reader on the order of approximation of each theory, a comparison among the pressure distribution given by the different

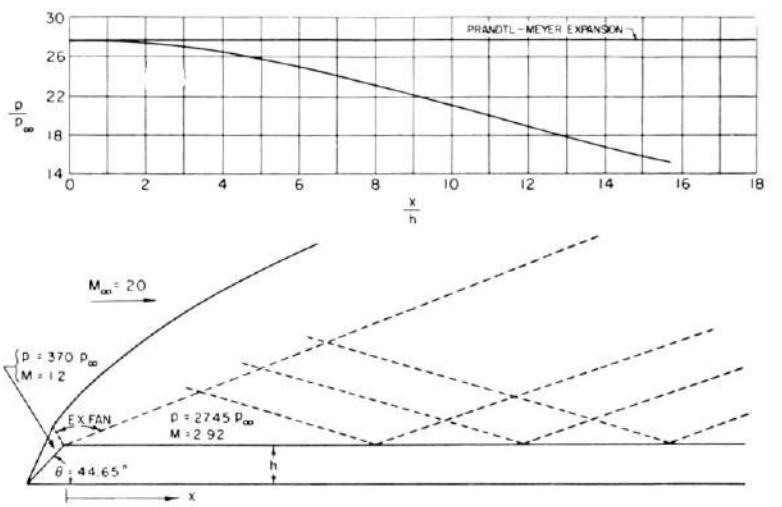

FIG. 8. Pressure distribution on a flat slab following a wedge as given by the Prandtl–Meyer expansion method and by the characteristics method[35].

methods of analysis for a sphere cylinder at $M=20$, and constant gas properties ($\gamma=1{\cdot}40$) is shown in Figs. 9(a) and 9(b).

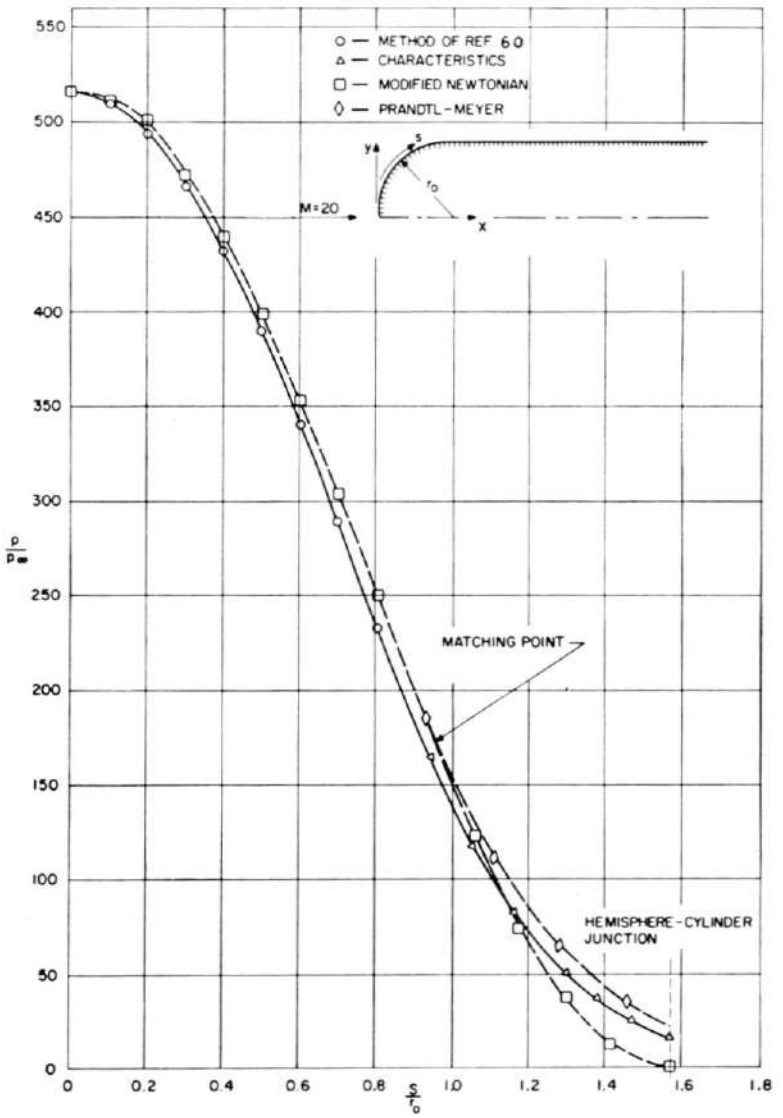

FIG. 9(a). Pressure distribution on a sphere cylinder at $M=20$ given by different analyses ($\gamma=1{\cdot}40$) (a) Front part of the body.

Figure 9(a) presents a comparison between the calculations performed in the elliptic region according to ref. 60 followed by a characteristic analysis with Newtonian theory, followed by a Prandtl-Meyer expansion. The point of tangency between the two methods has been chosen as the transition point between the two pertinent laws. The agreement between the two

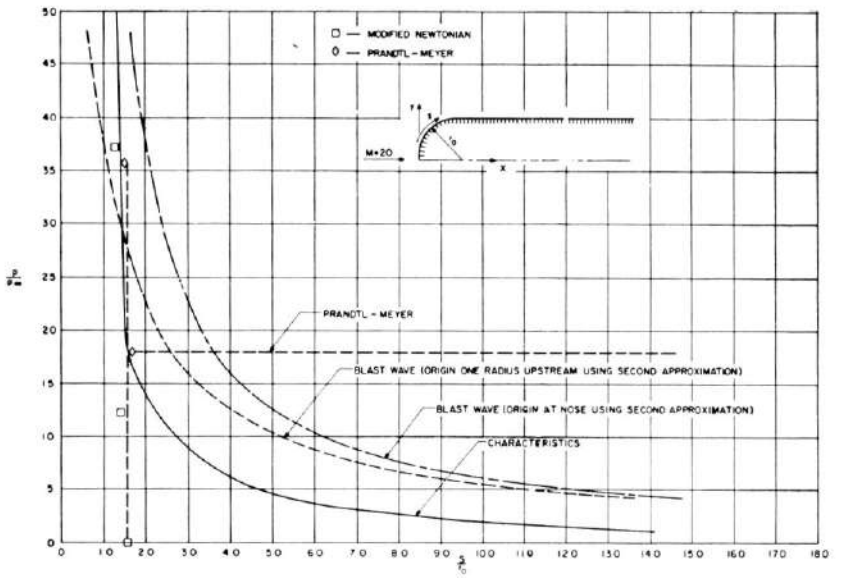

FIG. 9 (b) Cylindrical part.

analyses is very good. It must be noted that the Newtonian flow is independent of γ while the shock-expansion values are affected by the value of γ. The pressure distribution downstream of the body is shown in Fig. 9(b). The scales of the abscissa and ordinate have been changed. The blast wave theory gives values of pressure that are closer to the values calculated with characteristic theory than the Prandtl–Meyer approximation. However, as the absolute value of the pressure decreases the percentage error increases very rapidly. This error will affect any heat transfer calculation.

(b) *Pressure Distribution for Non-axially Symmetric Flow Fields*

Sharp-nosed bodies or cones at an angle of attack can be analyzed with known methods developed for supersonic flows. The Newtonian approximation for slender bodies has been also developed[72]. However, very little experimental or theoretical information is presently available for axially symmetric blunt bodies at an angle of attack. In refs. 73 to 75 experimental data are presented for the pressure distribution on blunted cones at angle of attack. The nose of the body is spherical and the elliptic region of the flow is for all cases on the spherical portion of the body. In this case the elliptic region is not influenced by the angle of attack effect and the flow in this part can be predicted by the Newtonian approximation and Prandtl–Meyer expansion. The stagnation point is on the radius parallel to free stream direction.

Downstream of the spherical region in the supersonic part of the flow, the effect of angle of attack is similar to the effect found for sharp-nosed bodies in supersonic flow. The experimental data of ref. 75 indicates that

the pressure distribution at a station along the body can be expressed in the form

$$p = p_0 + \alpha p_1 \cos \Psi + \alpha^2 p_2 + \alpha^2 p_3 \cos 2\Psi \tag{2.6}$$

where p_0 is the pressure at zero angle of attack. As an example, in Fig. 10 (a)

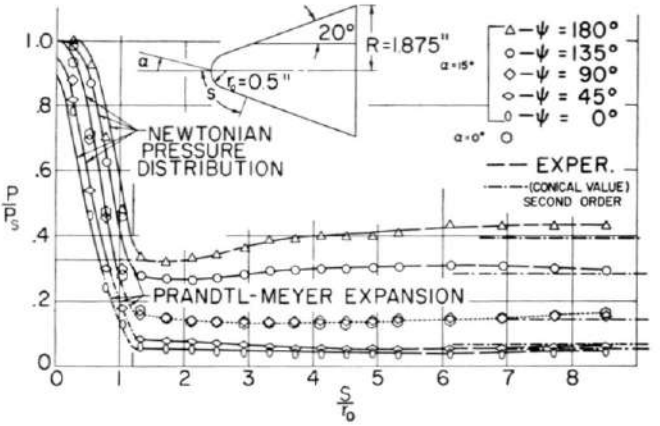

(a)

(b)

FIG. 10 (a). Pressure distribution on a blunted cone at 0° and 15° angle of attack at $M_\infty = 6$[75]. The body is a 20° blunt cone with hemispherical nose, $r_0/R = 0{\cdot}267$. (b) Shadow photograph of a blunted cone at 15° angle of attack at $M_\infty = 6$[75].

the pressure distribution on different meridian planes of a blunted cone at $\alpha = 15°$ is presented[75]. The pressure distribution given by Newtonian plus Prandtl–Meyer on the spherical part of the body and by Eq. (2.6) on

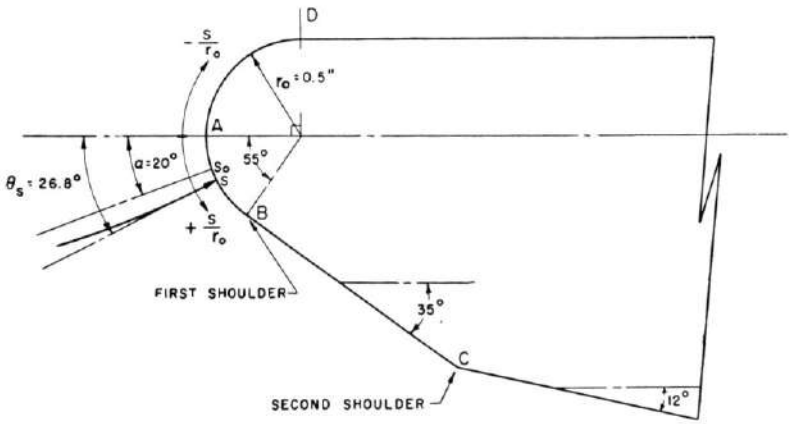

FIG. 11 (a). Two-dimensional body at an angle of attack.

the conical part are also presented. The values of p_1, p_2 and p_3 are obtained from the measured values at $\Psi=0°$, 90°, 180°. At large distance from the nose the flow is again conical. The values given by second order conical flow theory are also indicated in the figure.

The pressure distribution at $\Psi=90°$ and $\alpha=15°$ is practically the same as for $\alpha=0°$. For these types of bodies a first order rough estimate of the pressure distribution can be obtained from a very simple approach. The Newtonian approximation is used followed by a Prandtl–Meyer expansion on the spherical part. The asymptotic value for the cone is then used for the conical part. From these three values an approximate shape of the pressure distribution at 0 angle of attack is obtained.

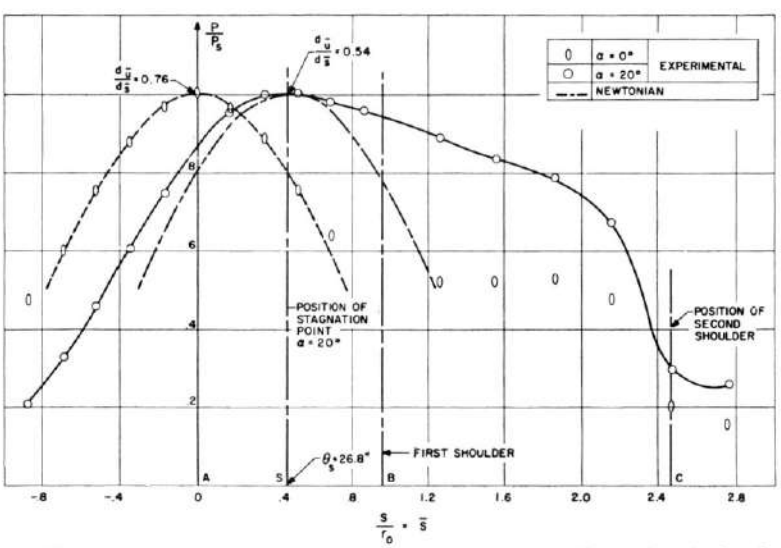

FIG. 11 (b). Pressure distribution at the nose of a two-dimensional circular nosed body at 0° and 20° angle of attack.

In the angle of attack case the pressure distribution at $\Psi=90°$ is taken equal to the pressure for the zero angle of attack case. At $\Psi=0°$ and $\Psi=180°$ the pressure is again obtained from Newtonian theory and then Prandtl–Meyer expansion on the spherical part of the nose while at a large distance from the nose second order conical flow theory for $\alpha \neq 0°$ is used. In this way a rough first-order approximation is obtained that can be useful for determination of forces.

It must be noted that the Newtonian flow and Prandtl–Meyer expansion approximation gives at the shoulder lower pressure values than the conical flow theory for large local cone angles. Therefore, the over-expansion found experimentally is also represented by this approach. The transition from the blunt nose region to approximately conical flow can be expected to take place in a length of the same order of the distance between the body and shock at the shoulder divided by the tangent to the local Mach angle of the conical body. The over-expansion on the plane $\Psi=180°$, affects the shock which in this plane is close to the body. Therefore, near the nose the shock is concave and then becomes tangent to the shock for the nose. In the plane $\Psi=0°$ the shock has monotonic curvature (Fig. 10(b)).

When the nose has a circular cross section and the angle of attack affects the elliptic region of the flow, then the position of the stagnation point cannot be determined directly from geometric considerations by assuming that it is at the point where the normal to the body surface is parallel to the free stream direction. In this case the pressure distribution along the body and the velocity gradient are strongly affected by non-symmetry. The same is true when the body is at an angle of attack and the body has a cross-section different from circular. The asymmetry can affect the heat transfer at the stagnation point. Consider for example the two-dimensional body shown in Fig. 11(a). Until the sonic point is on the circular portion of the body flow on the nose is symmetrical with respect to the stagnation point, which is on the radius parallel to stream direction. However, for larger angles of attack the sonic point moves outside of point B. In this case the position of the sonic point is determined by the position of point C or if the region BC is curved by the curvature of the region BC. The other sonic point will be still located in the region AD. Then the flow is nonsymmetrical and the stagnation point is not at the point S_0 on the radius parallel to the velocity direction but moves to a point S which is between S_0 and B (the curvature at B along BC has been assumed larger than along AB). Figure 11(b) gives the pressure distribution along the body for the case of $\alpha=0°$, and $\alpha=20°$. For the case of $\alpha=0°$, the Newtonian approximation is in good agreement with the experimental results. For $\alpha=20°$ the stagnation point is not on the radius parallel to the free stream direction ($\theta=20°$), but is at a position corresponding to 26·8°. The motion of the stagnation point is not included in the Newtonian approximation and the pressure distribution for $\alpha=20°$ differs from the Newtonian pressure distribution. The effect of this shift of the stagnation point is

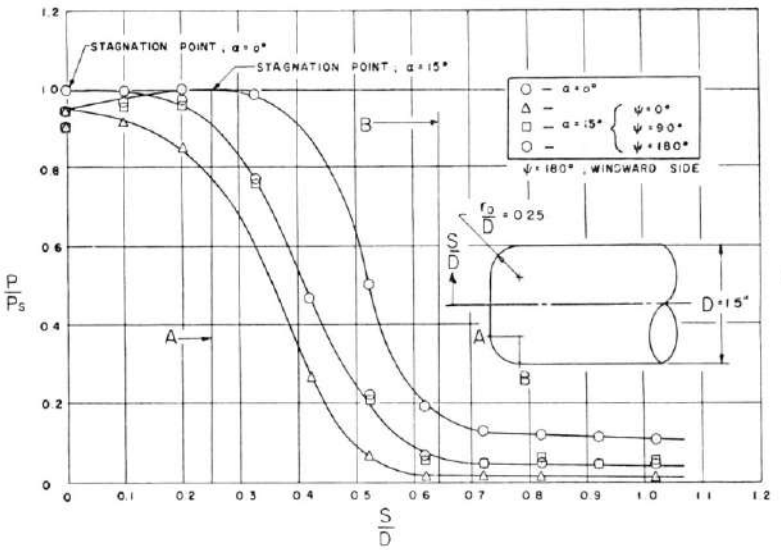

(a)

FIG. 12. Pressure distribution on a flat-nosed axially symmetric body at 0° and 15° angle of attack at $M_\infty = 6$.

(a) Pressure distribution in the plane $\Psi = 0°$, 90°, 180°.

(b) Pressure distribution near stagnation point $\alpha = 0°$ and $\alpha = 15°$ at $\Psi = 0°$, 45°, 90°, 135°, 180°.

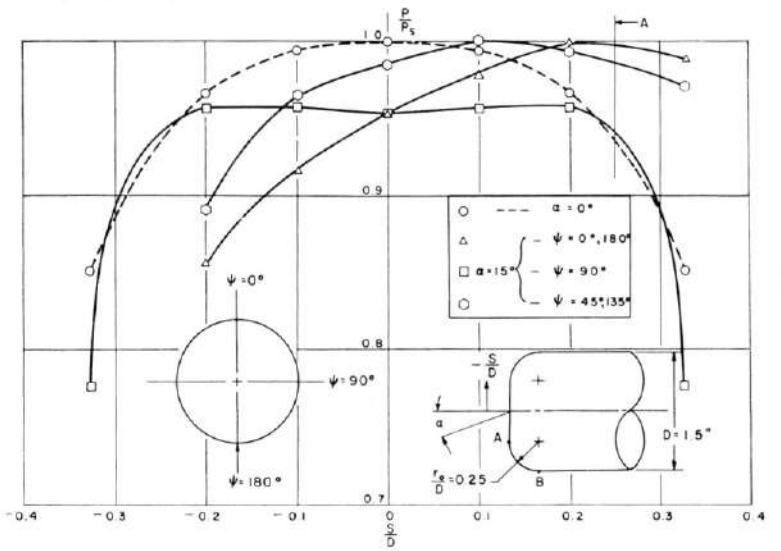

(b)

important because it changes the value of the pressure and velocity gradient at the stagnation point and, therefore, the value of the heat transfer. The nondimensional velocity gradient $d\bar{u}/d\bar{s}$ calculated from the experimental data for $\alpha = 20°$ is 0·54 in comparison with a value of 0·76 for the

case of $\alpha=0°$; therefore the heat transfer at the stagnation point for $\alpha=20°$ is of the order of 20% less than for the case of $\alpha=0°$, in spite of the fact that the radius at the stagnation point is the same. This effect can be of interest for practical applications on wing leading edges.

The nonsymmetry of the flow at the stagnation point exists also for axially symmetric bodies at an angle of attack[76]. Also, in this case the pressure distribution cannot be obtained analytically and must be determined experimentally. In Fig. 12(a) the pressure distribution measured on

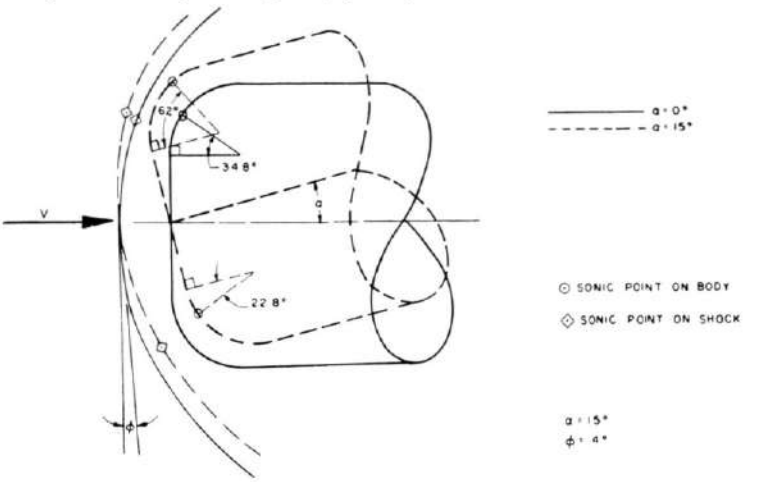

FIG. 12(c). Shock shapes for the flat-nosed bodies at $\alpha=15°$ and $\alpha=0°$ at $\Psi=0°, 180°$.

a flat-nosed body at $\alpha=0°$ and $\alpha=15°$ and $M=6$ is shown. Also in this case, where the angle of attack changes, the stagnation point moves and the pressure distribution changes. In Fig. 12(b) the pressure distribution in different meridian planes for the case of $\alpha=15°$ near the stagnation point is shown. In Fig. 12(c) the shapes of the shock for $\alpha=0°$ and $\alpha=15°$ in the planes $\Psi=0°$, 180° are shown. The distance of the shock from the axis of the body is the same for $\alpha=0°$ and $\alpha=15°$. The shape of the shock near the stagnation point is practically the same. However, the shock for $\alpha=15°$ rotates much less than the body (about 4°). The position of the sonic points on the shock and on the body is also indicated in Fig. 12c.

The heat transfer at the stagnation point can be determined from the considerations of ref. 78. The theoretical value of heat transfer at the stagnation point for $\alpha=15°$ is roughly equal to the value at $\alpha=0°$, if the experimental pressure distribution is used in the heat transfer analysis. The displacement of the stagnation point could probably be obtained from incompressible flow analysis. The incompressible irrotational flow for a flat disk gives a ratio of displacement r to diameter D of 0·20 for $\alpha=15°$ in comparison with the value of 0·19 given by the experiments.

A small amount of theoretical or experimental work is presently available for general three-dimensional flow. It can be expected that the Newtonian

theory type of solutions can probably be extended to the analysis of the subsonic region of blunt-nosed bodies without axial symmetry while conical or two-dimensional considerations can be used locally in the supersonic region. For this reason conical flow fields without axial symmetry can be of practical interest in hypersonic flow. Some experimental results of pressure distribution on an elliptical cone at 0°, 10° and 20° angle of attack and $M_\infty = 6$ are shown in Fig. 13. The cross section of the cone

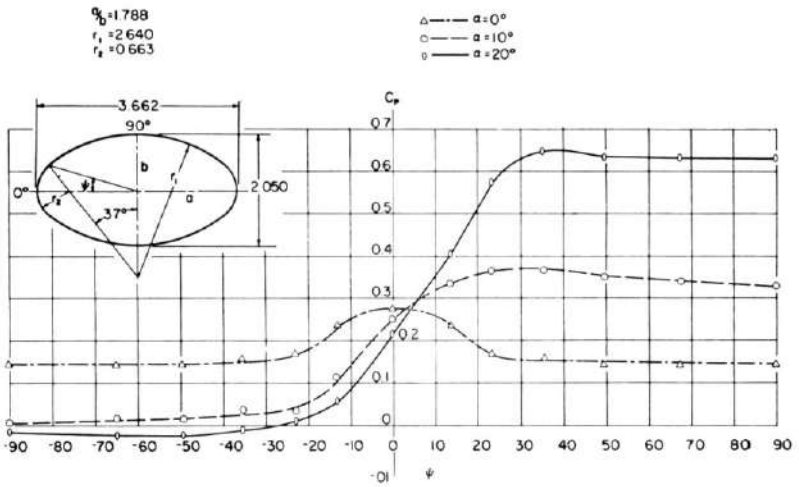

FIG. 13. Pressure distribution on an elliptical cone at $\alpha = 0°$, 10°, 20°, and $M_\infty = 6$.

has a ratio of the two principal axes equal to 1·788 and a ratio of the height H to equivalent radius $H/\sqrt{ab}$ equal to 3·315. The cross section has been approximated in the model construction by two circular arcs of different radii. A comparison of these experimental results with values obtained from different analyses is presently in process.

3. HEAT TRANSFER

(a) *Laminar Heat Transfer*

Heat transfer analyses and measurements for laminar boundary layers on axially symmetric or two-dimensional bodies are at present available. The theoretical results agree well with experimental results (see, for example, refs. 75, 77, 79). The heat transfer at the stagnation point can be analyzed with the method of ref. 23, while the variation of heat transfer along the body can be approximated with sufficient accuracy by the method of ref. 24. As an example in Fig. 14[75] a comparison between theoretical and experimental results for a blunted nose are shown. In the analysis the actual measured pressure distribution has been used. The stagnation point has been calculated as in ref. 23 and the distribution as in ref. 24. The variation of the Nusselt number with Reynolds number for laminar

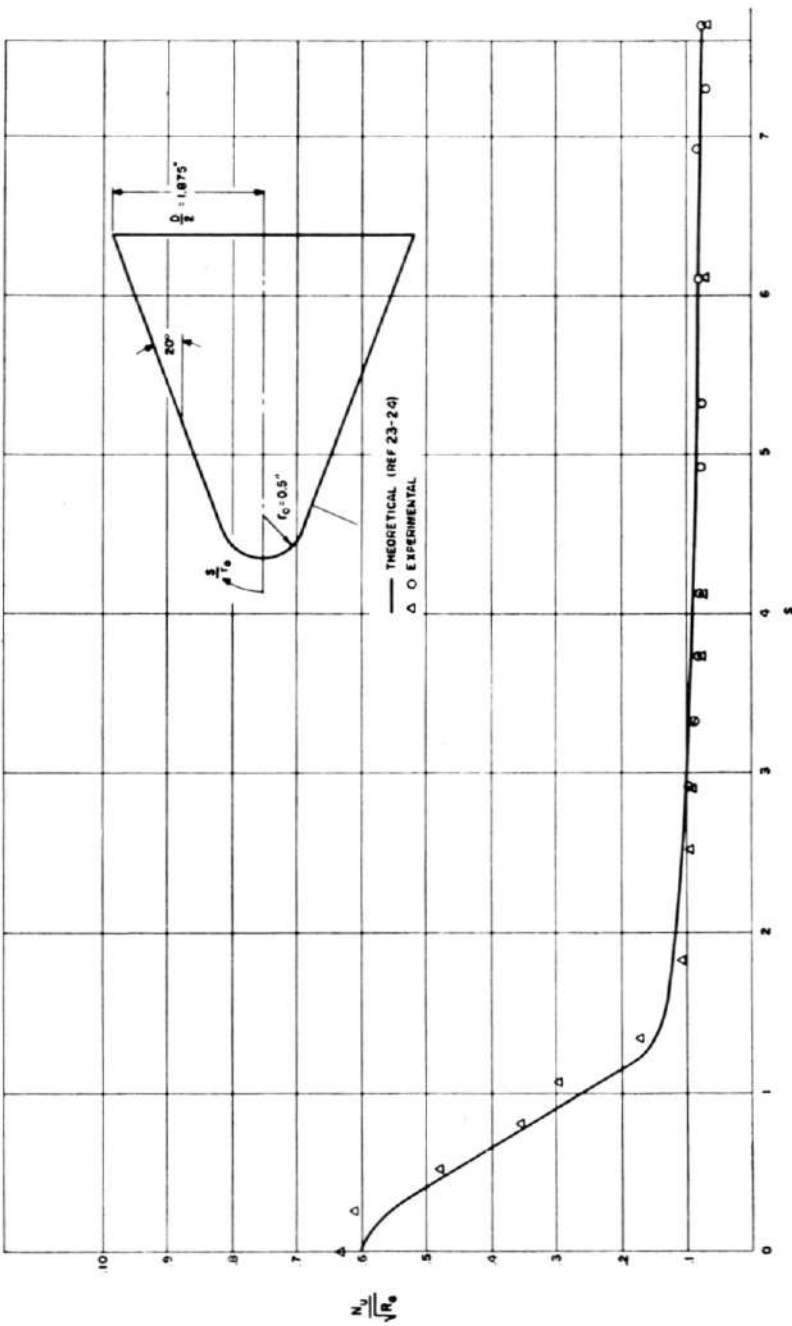

FIG. 14. Comparison between theoretical and experimental laminar heat transfer distribution at the surface of a 20° blunted cone at $\alpha = 0°$ and $M_\infty = 6$ [75].

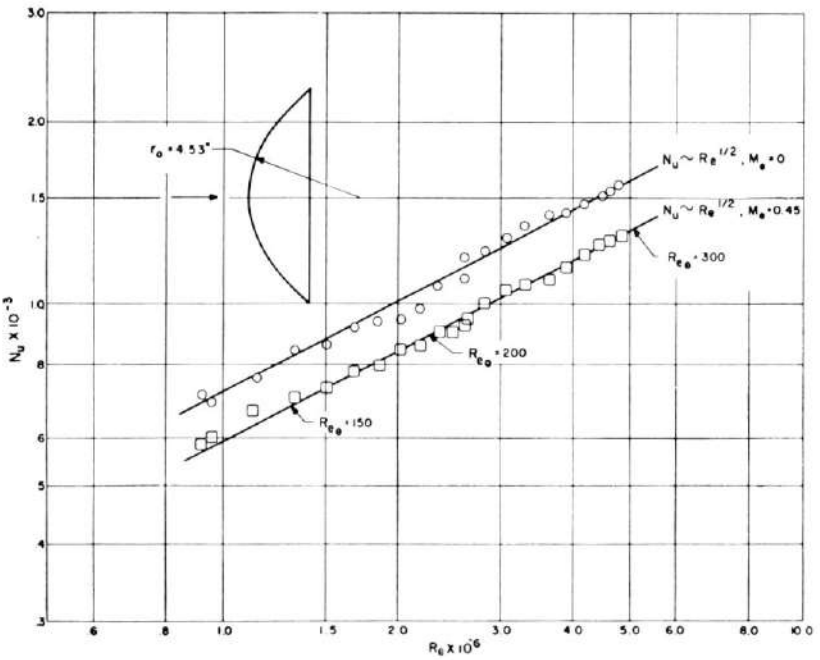

FIG. 15. Nusselt number as a function of Reynolds number for laminar boundary layer in the presence of a pressure gradient.

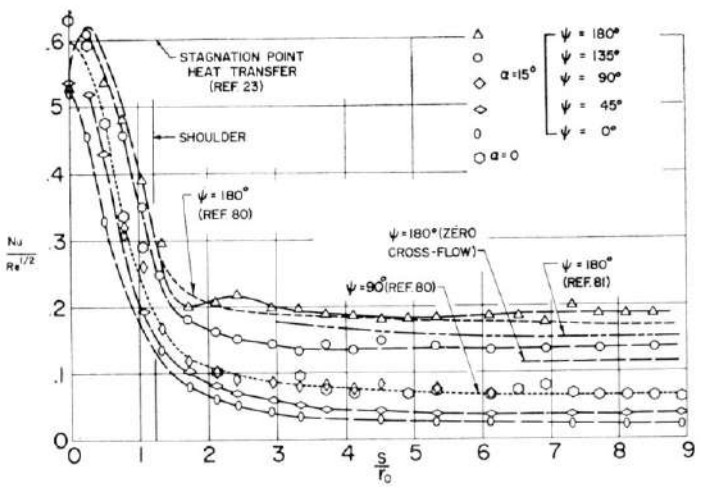

FIG. 16. Laminar heat transfer distribution on the blunt cone at 0° and 15° angle of attack at $M_\infty = 6$. (The body is a 20° blunt cone, with hemispherical nose $r/R = 0{\cdot}267$.)

boundary layer in the presence of pressure gradient is well represented by the expression

$$Nu = KR_e^{\frac{1}{2}}$$

(This relation is valid only if large entropy gradients do not affect the boundary conditions outside of the boundary layer; I will show later that large entropy gradients outside the boundary layer alter this relation.) In order to illustrate this point in Fig. 15 experimental results obtained at the Polytechnic Institute of Brooklyn with the shroud technique are presented for the stagnation point on a blunt body and for a point in the subsonic region.

Less detailed information is available for three-dimensional laminar boundary layer. Theoretical work in this direction has been presented in refs. 78 and 80. A small amount of experimental work is presently available.

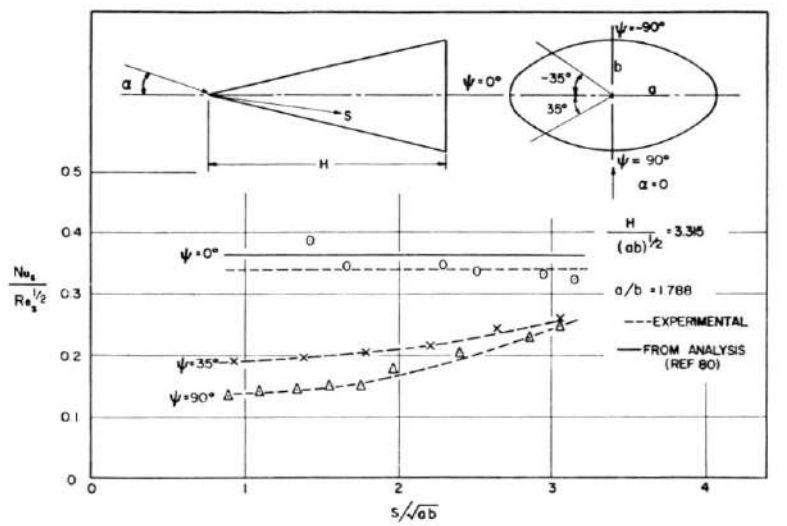

FIG. 17. Heat transfer on an elliptical cone at $\alpha = 0°$ and $M_\infty = 6$.

In Fig. 16 the heat transfer on a 20° blunted cone at 15° angle of attack is presented[75]. For comparison with the values given by the method of ref. 80 for the meridian planes $\Psi = 180°$ and $\Psi = 90°$ are shown in the figure. The method cannot be applied at $\Psi = 0°$. Theoretical values obtained by neglecting the effect of the crossflow on the boundary layer but considering the actual pressure distribution and values given by the analysis of ref. 81 for a cone at an angle of attack having equal local conditions are also shown in Fig. 16. In Fig. 17 heat transfer data for three meridian planes of an elliptical cone at $M_\infty = 6$ and $\alpha = 0°$, are pre-

sented. The corresponding pressure distribution has been presented in Fig. 13. The theoretical values of the $Nu_s/Re_s^{\frac{1}{2}}$ given by the analyses of ref. 80 and ref. 81 for $\alpha=0°$ and $\Psi=0°$ are also shown in Fig. 17. The value of $Nu_s/Re_s^{\frac{1}{2}}$ in the plane $\Psi=0°$ and $\alpha=0°$ where the crossflow is zero, is constant along the cone; however, this value varies with the non-dimensional distance $s/\sqrt{ab}$ for other conditions. This variation is not predicted by the simplified theories presently available. Possible explanation of this variation will be discussed later.

(b) *Transition and Turbulent Heat Transfer*

Little theoretical and experimental information is available for turbulent heat transfer. A detailed discussion of the different type of analyses has been given in ref. 82, where experimental results have also been presented. From these and other experimental investigations available[83], it appears that the Nusselt number for turbulent boundary layer with pressure gradient varies with the Reynolds number according to the expression:

$$Nu=KRe^{4/5}$$

A typical curve showing Nusselt number as a function of Reynolds

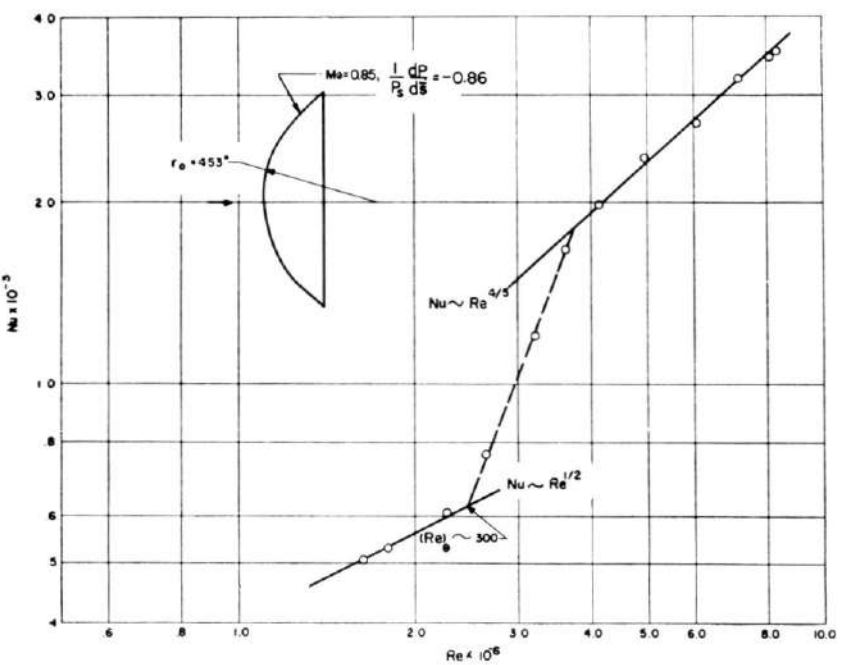

FIG. 18. Nusselt number as a function of Reynolds number for laminar transitional and turbulent boundary layer in the presence of pressure gradient.

number for laminar transitional and turbulent boundary layer is shown in Fig. 18. The curve presented corresponds to a point in the subsonic region of the body. The transition Reynolds number referred to the momentum thickness Re_θ is of the order of 300. The data have been obtained at the Polytechnic Institute of Brooklyn by means of the shroud technique. Again the presence of large entropy gradients outside the boundary layer can affect this relation.

The effect of pressure gradient has been considered by several authors and a critical comparison of different theories has been presented in ref. 82. All the analyses available assume that the skin friction coefficient is given by the flat plate skin friction law with corrections for compressibility and heat transfer[84–86]. The flat plate method assumes that the local conditions are the fundamental parameters on the heat transfer phenomena, and gradients in the stream directions do not need to be considered; then flat plate local conditions can be used. As conditions for evaluating the fluid properties, two alternatives appear reasonable, namely, the "reference enthalpy" and the "external conditions". Other analyses try to take into account the effect of variable pressure on the growth of the boundary layer. The comparison of ref. 82 indicates that, for the data available, the agreement with experimental results could be obtained best by the simplest type of analysis wherein the flat plate turbulent heat transfer corresponding either to reference enthalpy or to local external conditions is used. The more refined analyses that take into account pressure gradients tend to give results in poorer agreement than the flat plate type of analysis. Recently

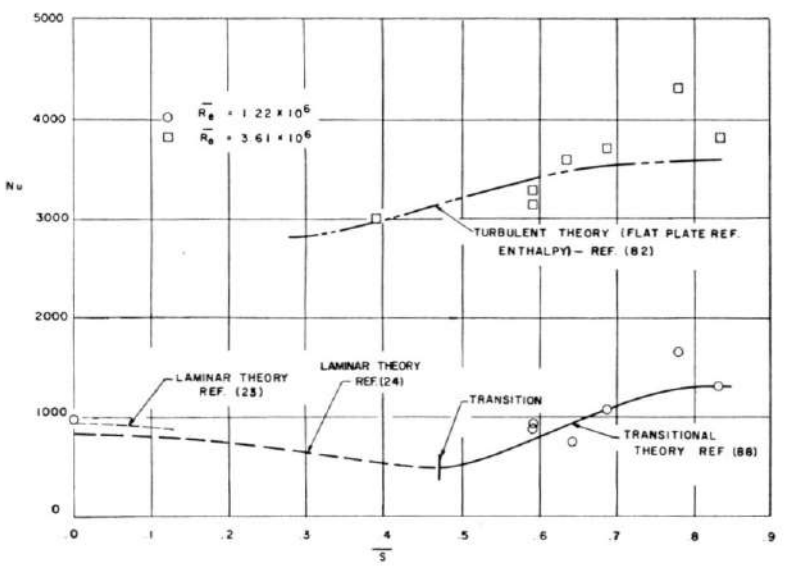

FIG. 19. Laminar transitional and turbulent heat transfer distribution on a blunt body for two Reynolds numbers.

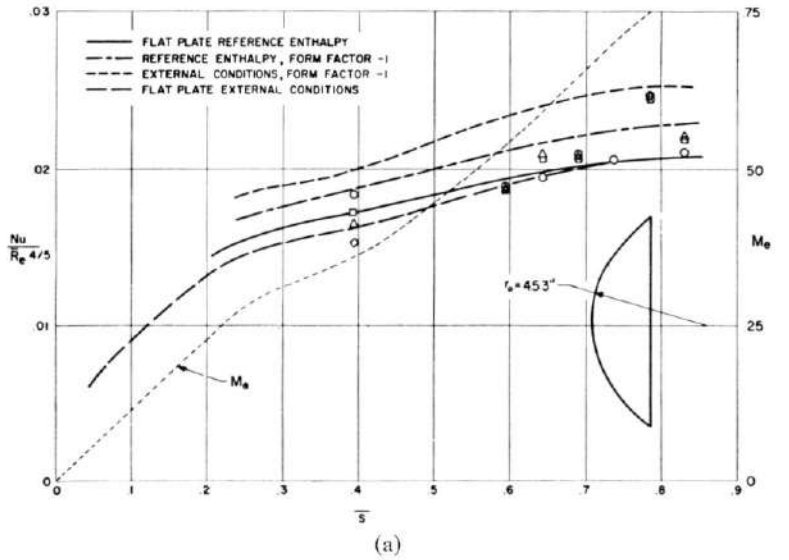

(a)

FIG. 20. Comparison between experimental and theoretical values of turbulent heat transfer in the presence of pressure gradient as a function of distance along the body.

(a) Spherical body; (b) blunted cone.

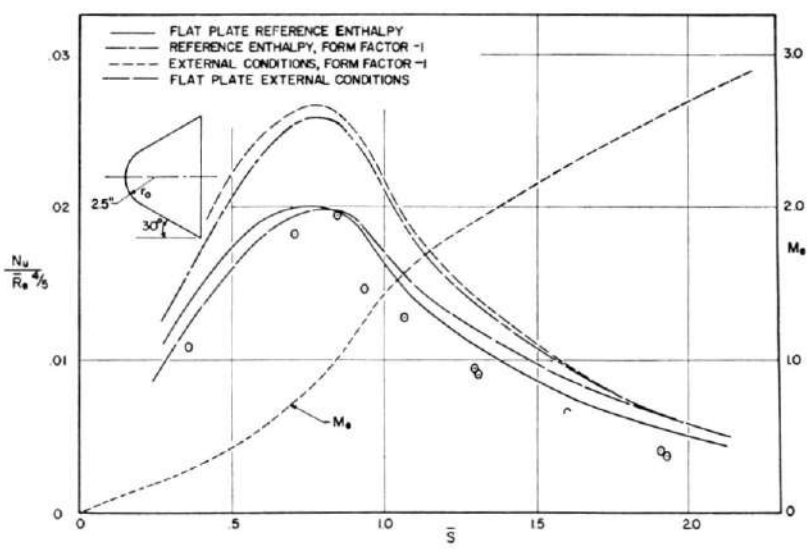

(b)

this problem has been reconsidered at the Polytechnic Institute of Brooklyn[87] and it has been shown that better agreement could be obtained between experimental values and the more rational analyses when a form factor equal to -1 is assumed for boundary layer profiles. With this assumption the effects of pressure gradients in Reynolds analogy disappears; however, the effects of the variable pressure on the boundary layer growth are considered. A comparison between experimental values obtained with the shroud technique and this analysis are shown in Figs. 19 and 20. Figure 19 presents the Nusselt number Nu (referred to the nose radius and stagnation conditions) as a function of position along a spherical body for two different Reynolds number Re. For both sets of data transition occurs on the body; the test corresponding to higher Reynolds number has a region of completely developed heat transfer. For blunt bodies transition from laminar to turbulent is gradual, and a transitional boundary layer covers a large and important part of the body surface.

An estimate of transitional heat transfer has been proposed in ref. 88. A comparison between experimental data and the values obtained by the methods of refs. 23 and 24 for the laminar part, ref. 88 for the transitional and flat plate external conditions for the turbulent part, is also shown in Fig. 19. Figure 20 presents a comparison between experimental data and data given by different theories on the front part of a spherical body (Fig. 20(a)) and on a blunted cone (Fig. 20(b)). The experimental data of Fig. 20(a) are obtained from ref. 87. The quantity $Nu/Re^{4/5}$ is plotted as a

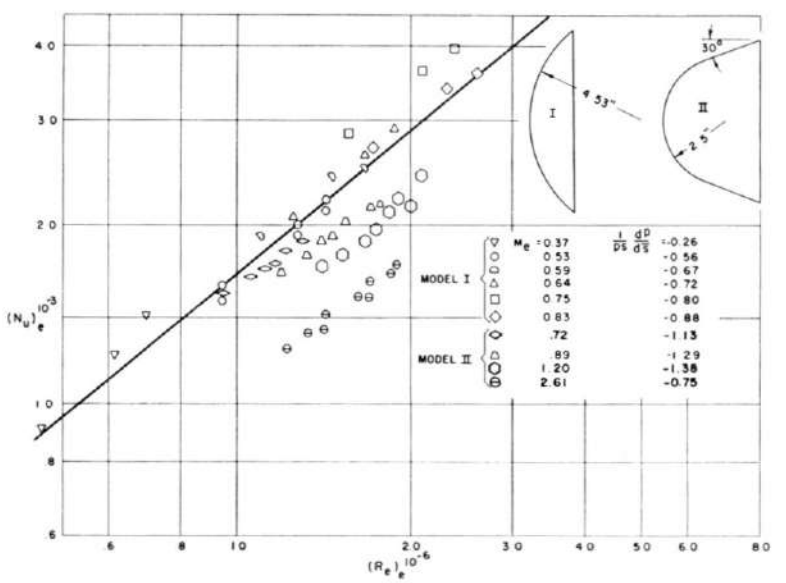

FIG. 21. Comparison between experimental and flat plate turbulent heat transfer in the presence of pressure gradient.

function of the non dimensional distance $\bar{s}$. Results of different analyses are presented; in the analyses the form factor has been assumed equal to —1. As additional information the Mach number distributions as function of $\bar{s}$ is also given.

A different comparison between experimental turbulent heat transfer data and theoretical data is presented in Fig. 21. In this figure the Nusselt number referred to local external conditions $(Nu)_e$ is plotted as a function of local Reynolds number for different positions on the two bodies of Figs. 20(a) and 20(b). The positions have been selected to cover a large range of local Mach numbers and local pressure gradients. The values of Mach numbers and pressure gradients are given in the figure. The analysis based on flat plate external conditions gives the $(Nu)_e$ as a unique function of $(Re)_e$. This relation is also shown in the figure as a continuous line. The agreement between experimental and theoretical results is good for subsonic flow. These results show larger discrepancy (of the order of 25%) in the supersonic region.

4. ENTROPY EFFECTS

The largest part of the work in boundary layer theory has followed the direction of trying to extend, simplify and modify boundary layer theory already developed for low speed or supersonic aerodynamics. In this process only few of the new parameters introduced by the hypersonic flow have been considered in detail, as for example, real gas effects. One characteristic of the hypersonic flow is the possibility of existence of large shear layers because of the presence of highly curved shocks. The large entropy gradients that can exist in hypersonic flow can have large effects on the heat transfer of the body and introduce new parameters in the boundary layer theory, in the stability theory, and open new directions on the possibility of reducing the heating problems. All these effects are important and deserve more attention.

In order to illustrate the importance of interference between boundary layer and entropy gradient consider the flow field produced by a blunted cone moving at hypersonic speed as sketched in Fig. 22. The shock at the nose is a curved shock. At some distance from the nose the flow is essentially conical and the pressure along the body is constant and equal to the pressure on a sharp cone. However the boundary layer on the body differs from the boundary layer at the surface of the cone, since the boundary conditions outside of the boundary layer are different; the velocity and density are lower, the static temperature is higher, and the gradient of velocity $\partial u/\partial y$ is not zero. The streamline at the outer edge of the boundary layer is generated at the curved portion of the shock and not at the conical part of the shock, and for given static pressure has much lower stagnation pressure than for the case of the cone. At the same time there exists an entropy gradient normal to the streamline which changes the boundary conditions. Both effects were discussed briefly for the first time in ref. 89.

Effects of small entropy gradients have been investigated in refs. 90, 91 and 92. However, the effect of entropy changes and large entropy gradients have not been considered in detail.

In order to obtain some order of magnitude of these effects it is convenient to discuss them separately. The presence of a velocity gradient $\partial u/\partial y$ at the outer edge of the boundary layer is important only if this gradient is of the same order as the velocity gradients $\partial u/\partial y$ produced by viscous effects in the boundary layer; these in turn are a function of Reynolds number. Therefore, some indication of the range of flight conditions, where velocity gradient produced by entropy gradient can be important, can be obtained by comparing the velocity gradients produced by the entropy field with the gradients produced by viscous forces. In the

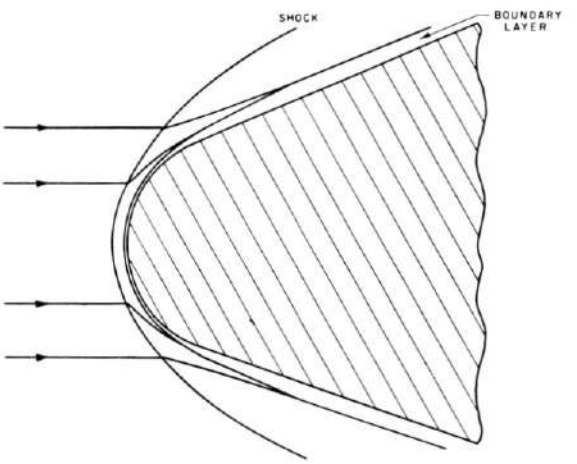

FIG. 22. Schematic representation of entropy gradients and boundary layer interference.

blunted cone of Fig. 22 the shock for $M=20$ is close to a parabolic shock that at some distance becomes tangent to a conical shock. For this shape of the shock and for this type of analysis the $\partial u/\partial y$ as function of y outside the boundary layer can be considered to be constant in the region of the parabolic shock and then zero in the conical region. In this case a vortical layer can be defined having constant mass flow equal to the mass going through the parabolic part of the shock and variable thickness; the velocity gradient existing in this vortical layer increases moving along the conical surface because the thickness of the layer decreases. The value of the velocity gradient in the boundary layer at the wall is a function of flight altitude and boundary layer thickness and can be obtained from boundary layer theory. The values of $\partial(u/u_c)/\partial y$ at the wall and at the outer edge of the boundary layer have been calculated for a 20° blunted cone at $M=20$ and different flight height. The results are presented in Fig. 23. The

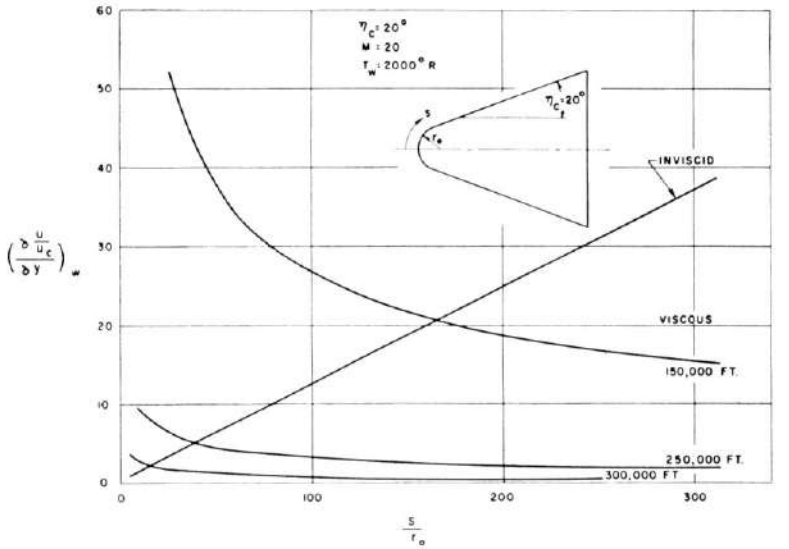

FIG. 23. Comparison between the velocity gradient produced by the entropy layer and the velocity gradient produced by the boundary layer at the wall for different flight altitudes. Flight Mach number = 20, wall temperature $T_w = 2000°$R.

value of u_c is the velocity at the cone surface for inviscid flow, r_0 is the nose radius and s the distance along the body.

For very high altitude flight of the order of 250,000, 300,000 ft, the two velocity gradients given by the viscous forces and by the entropy gradients are of the same order even for small values of s/r_0; therefore in this case it does not seem possible any more to divide the flow field in a viscid and inviscid flow region. However, for lower altitudes of flight, and small values of s/r_0 the ratio of the two gradients is small; therefore the effect of velocity gradient due to the entropy gradient is probably small. The results of refs. 90, 91 and 92 tend to indicate that this is the fact.

For low altitude of flight the second effect is probably more important. The flow entering the boundary layer comes from the region of the strong shock; therefore, for small mass flow in the boundary layer in the region of constant pressure it can be assumed that the conditions outside of the boundary layer are defined by normal shock stagnation pressure recovery and static pressure equal to the conical pressure. When the heat transfer determined with this external condition is compared with the heat transfer on a cone with the same cone angle, it is found that because of the loss of stagnation pressure across the normal shock, the heat transfer on the blunted cone is appreciably less than on the cone, especially if the angle of the cone is small.

A comparison between the heat transfer on a cone and on a blunt cone for turbulent boundary layer at $M = 15$ and 60,000 ft of altitude is shown in Fig. 24. The differences between the two values are large and are due to

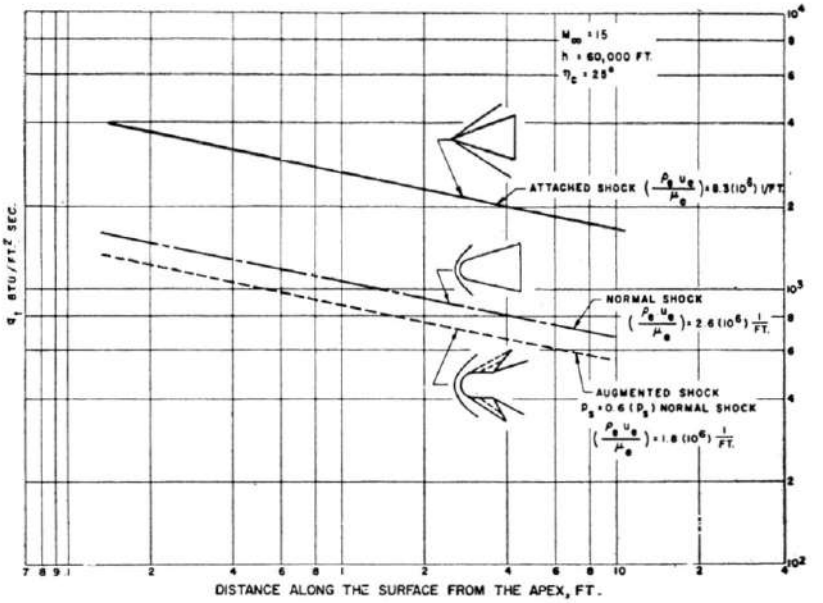

FIG. 24. Comparison among turbulent heat transfer values along a sharp 25° cone, a blunt 25° cone, and a blunt 25° cone with one additional bump. Flight conditions $M_\infty = 15$, altitude 60,000 ft.

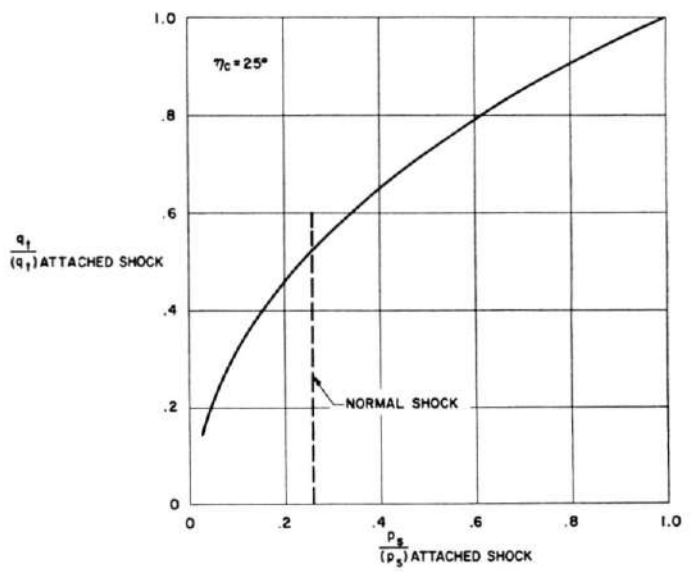

FIG. 25. A dimensional turbulent heat transfer coefficient at the surface of a 25° conical body as a function of stagnation pressure outside the boundary layer for $M_\infty = 15$ and 60,000 ft and constant static pressure.

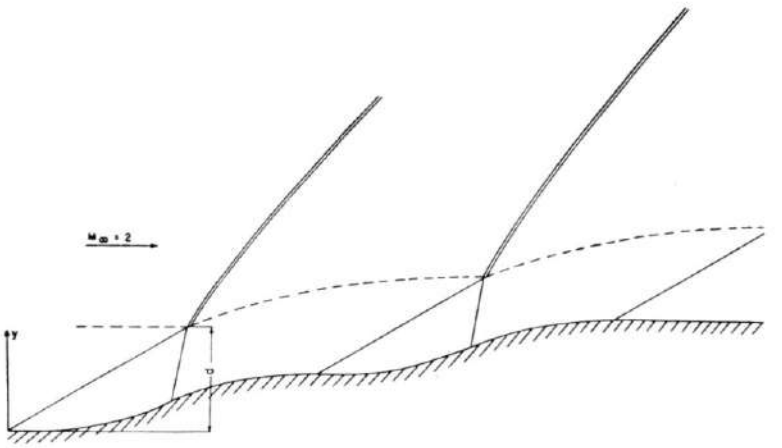

(a)

FIG. 26. (a) Schematic design of surface bumps for local increase of entropy outside of the boundary layer; (b) Distributions of flow properties and heat transfer ratios downstream of the bumps.

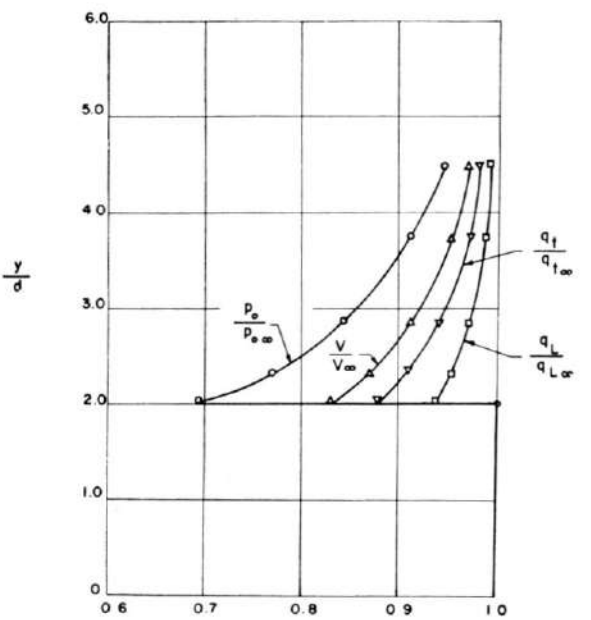

(b)

the differences in entropy outside the boundary layer and thus to the changes in the value of $\rho_e u_e/\mu_e$ outside the boundary layer.

Because of the large effects of the variation of entropy a new possible approach for decreasing the heat flux on the body can be considered. If the value of the entropy in the flow immediately outside the boundary layer can be increased by local changes, then a reduction in heat flux would be produced. In Fig. 24 an additional curve is presented corresponding to a body where the entropy outside the boundary layer is increased locally by introducing an indentation on the body. The indentation produces an expansion followed by a compression, which, at small distances, generates a localized shock. This shock increases entropy and decreases the heat transfer downstream of the indentation. In Fig. 25 the turbulent local heat flux on the conical part is plotted as a function of stagnation pressure existing outside of the boundary layer for the same flight conditions. The reductions that could be obtained by decreasing the stagnation pressure outside of the boundary layer are important. Real gas is assumed in the analysis.

The decrease in stagnation pressure outside of the boundary layer can be obtained with very localized changes on the body shape without changing the general shape of the body. Assume, for example, a bump or a series of bumps are introduced locally at the surface of the body, as shown in Fig. 26(a). The bumps produce gradual compressions at the surface and strong shocks in a very limited region of the flow. Then the entropy can be increased locally and the heat transfer decreased. In Fig. 26(b) the ratio p_0/p_{0_∞} between the stagnation pressure downstream of the bumps and upstream of the bumps is indicated as a function of local position. The upstream local Mach number is equal to 2. The variation of local velocity for the same static pressure downstream and upstream of the bumps is given by the ratio u/u_∞. The effect of the variation of external conditions on turbulent or laminar heat transfer (subscripts t and L, respectively) is given by the ratio q_t/q_{t_∞} and q_L/q_{L_∞}. In the determination of these ratios the effects of $\partial u/\partial y$ outside the boundary layers have been neglected.

In Fig. 27 some experimental results obtained at $M_\infty = 6$ proving this effect are presented. A conical body with two different noses has been tested. The two noses are a conical tip and a spherical nose. The measured pressure along the conical body at some distance from the tip is equal in the two cases. However, the heat transfer is largest for the conical tip which produces the least entropy raise and lowest for the blunted nose. The boundary layer is laminar for both tests, and the measured differences are of the order of 18%. Theoretical values differ for these conditions by about 20%.

The possibility of large entropy change existing at hypersonic speed could introduce a new mechanism for transition due to roughness. Assume that the bump discussed before is small, such that the entropy gradients

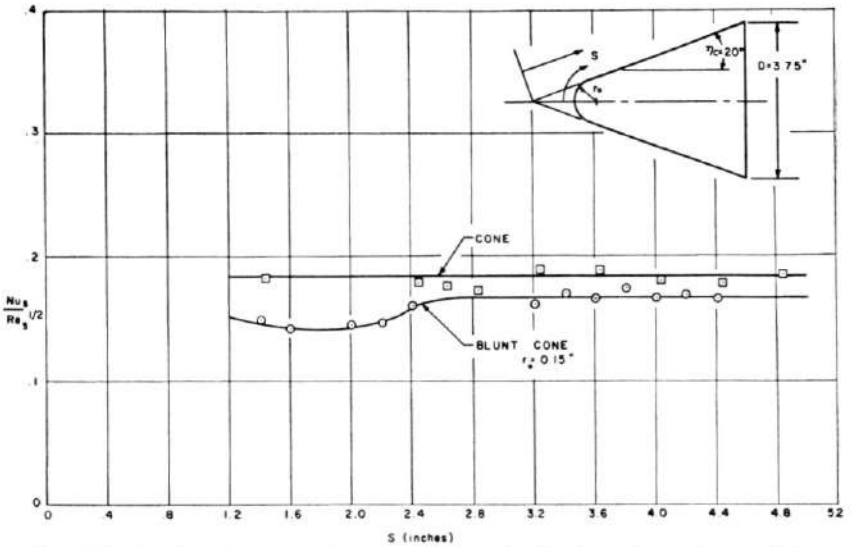

FIG. 27. Laminar heat transfer on a 20° conical body with conical or blunt tip at $M_\infty = 6$.

are within the boundary layer thickness. Because a large part of the boundary layer flow is supersonic large entropy variations could occur in the boundary layer because of the bump. In the immediate vicinity of the bump the pressure is not constant normal to the surface. Thus the boundary layer theory is not strictly valid there. However, the theory would again become valid downstream of the bump where the pressure becomes uniform. The entropy raise can change the boundary profile as shown schematically in Fig. 28 and affect transition.

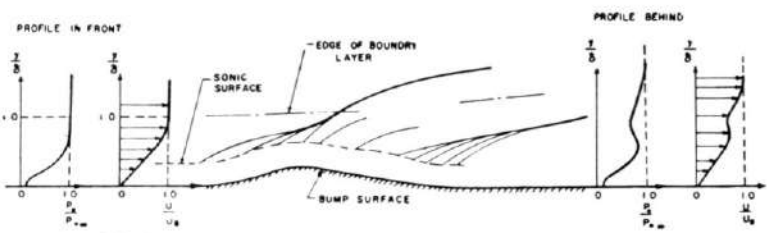

FIG. 28. Schematic effect of a bump on boundary layer profiles.

As the boundary layer grows the entropy outside of the boundary layer tends to decrease because of the presence of the curved shock in front and the velocity outside the boundary layer tends to increase. Because of the large changes of the external conditions, a new parameter must be considered in the boundary layer analysis, that is, the mass flow entrained in the boundary layer. The changes of external conditions are large, especially for axially symmetric bodies and, in many cases, cannot be neglected.

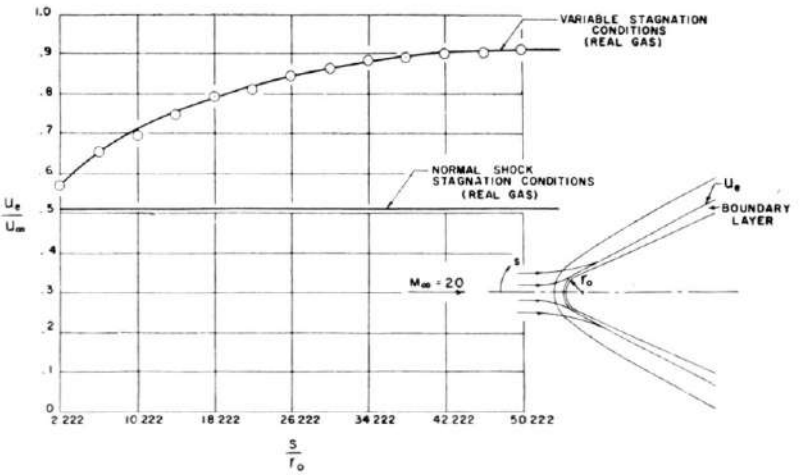

FIG. 29. Distribution of velocity outside the boundary layer along a 20° blunt cone at $M_\infty = 20$ and 100,000 ft altitude, determined from normal shock stagnation conditions and from shock conditions corresponding to correct mass flow.

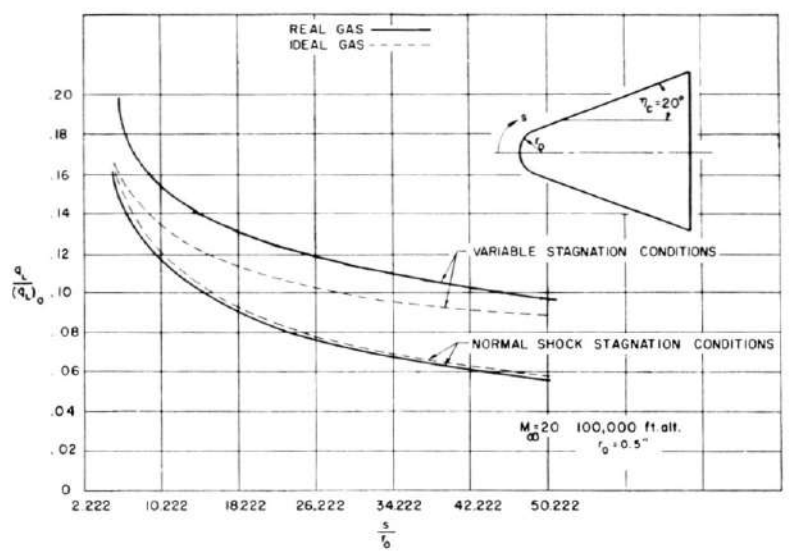

FIG. 30. Approximate theoretical laminar heat transfer distribution along a 20° blunt cone at $M_\infty = 20$ and 100,000 ft altitude for the case of constant or variable entropy outside the boundary layer.

In order to obtain an order of magnitude of such effects a rough approximate analysis has been performed for the boundary layer on a blunt cone at $M=20$. Some of the results of such analysis are shown in Figs. 29 and 30. In Fig. 29 the velocity outside the boundary layer is plotted as a function of distance along the body for the condition of constant entropy outside of the boundary layer, and corresponding to normal shock in front, and for the condition where the actual entropy existing outside the boundary layer is used to determine the velocity. The pressure distribution is assumed equal in both cases. The velocity at stations far from the nose is quite different for the two cases. The differences are reflected in the local values of the heat transfer. Results of a rough analysis of laminar heat transfer on the blunt cone considered in Fig. 29 at $M=20$ are shown in Fig. 30. The procedure followed in the analysis is similar to the method of ref. 24. It can be shown that some of the additional terms appearing in the momentum equation for the case of variable entropy are small for the example considered; therefore an analysis along the line of ref. 24 with the required modifications still gives reasonable first order predictions. Large differences are found between the isentropic and the variable entropy case for all the conditions considered. In Fig. 30 results of a calculation where variable entropy and real gas effects are considered is also presented. The entropy change is altered by real gas effects. In all cases the boundary layer is assumed to be laminar. Larger differences due to entropy can be expected for turbulent boundary layers.

Experimental results confirm the importance of these entropy gradients. In Fig. 31 the results of laminar heat transfer measurements performed at $M=6$ on a family of blunted cones at different Reynolds number is presented. The figure shows the ratio of Nusselt number to Reynolds number at one-half power, as a function of the distance along the body divided by the nose radius and by Reynolds number at one-half power. Both Nusselt number and Reynolds number are referred to the length s, distance from the nose. The choice of this co-ordinate system permits us to obtain some indication of the entropy effects.

For a cone the $Nu_s/Re_s^{\frac{1}{2}}$ is a constant and independent of the distance s. This value is also practically constant on the conical part of a blunted cone when the entropy gradient effects are neglected. The entropy at any point of the flow field depends on the position of the intersection of the streamline passing through the point considered with the front shock. If r is the radius of this intersection, then the mass flow contained inside the streamtube defined by this streamline is

$$m=\rho_1 V_1 r^2$$

The entropy at a given point of the shock is a function of r/r_0 where r_0 is the radius of the nose; therefore the entropy is a function of the quantity $m/\rho_1 V_1 r_0^2$. The mass flow entering the boundary layer on the conical part of the blunt body at some distance from the nose, can be assumed to be

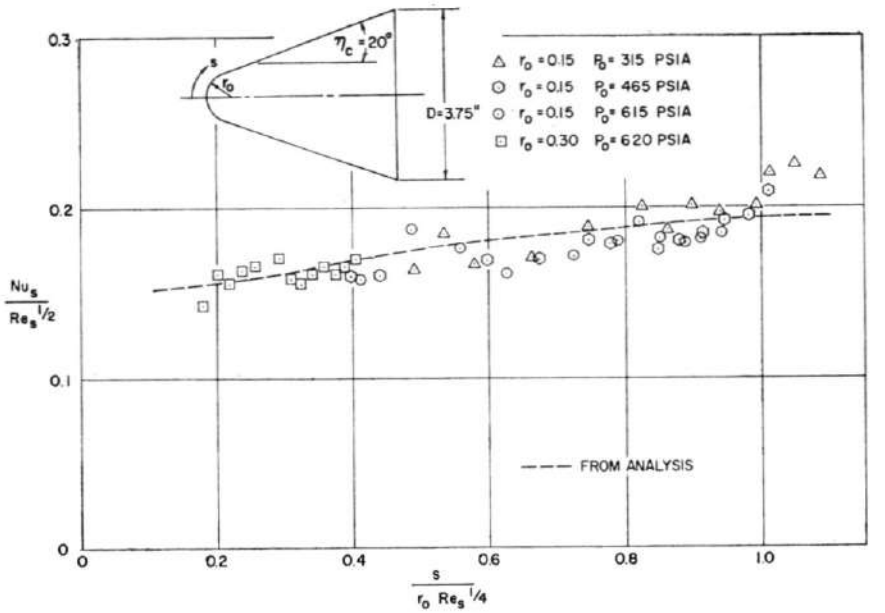

FIG. 31. Experimental determination of entropy variation effects: $Nu_s/\sqrt{Re_s}$ as a function of $s/r_0\ Re_s^{\frac{1}{4}}$.

close to the mass flow entering the boundary layer on a conical flow; therefore, it can be expressed approximately as

$$m_b = Ar\,\delta\rho_e u_e = A\sqrt{Re_s}\,r\mu_e$$

where A is a constant, δ the boundary layer thickness. Two points on the body tested at different stagnation conditions have the same entropy outside of the boundary layer when $m_b/\rho_1 V_1 r_0^2$ is the same or when $s/r_0\ Re_s^{\frac{1}{4}}$ is the same. If $(Nu/\sqrt{Re})_s$ is independent of s/r_0 then by plotting the value of $(Nu/\sqrt{Re})_s$ as a function of $s/r_0\ Re_s^{\frac{1}{4}}$ the effect of entropy can be indicated.

The data presented in Fig. 31 indicate the effects of entropy changes. For low values of $s/r_0\ Re_s^{\frac{1}{4}}$ the $Nu_s/\sqrt{Re_s}$ is approximately constant with $s/r_0\ Re_s^{\frac{1}{4}}$; however, for large values of $s/r_0\ Re_s^{\frac{1}{4}}$ the value of $Nu/\sqrt{Re_s}$ increases. For comparison a curve obtained analytically is also shown.

The laminar boundary layer in the absence of entropy variations indicates that the value of $Nu/\sqrt{Re}$ at a given station is independent of the Reynolds number. The simple analysis presented above indicates that the entropy outside of the boundary layer at a given station s/r_0 changes when the Reynolds number changes. This implies that the quantity $Nu/\sqrt{Re}$ will change with Reynolds number if the entropy effects are important. In

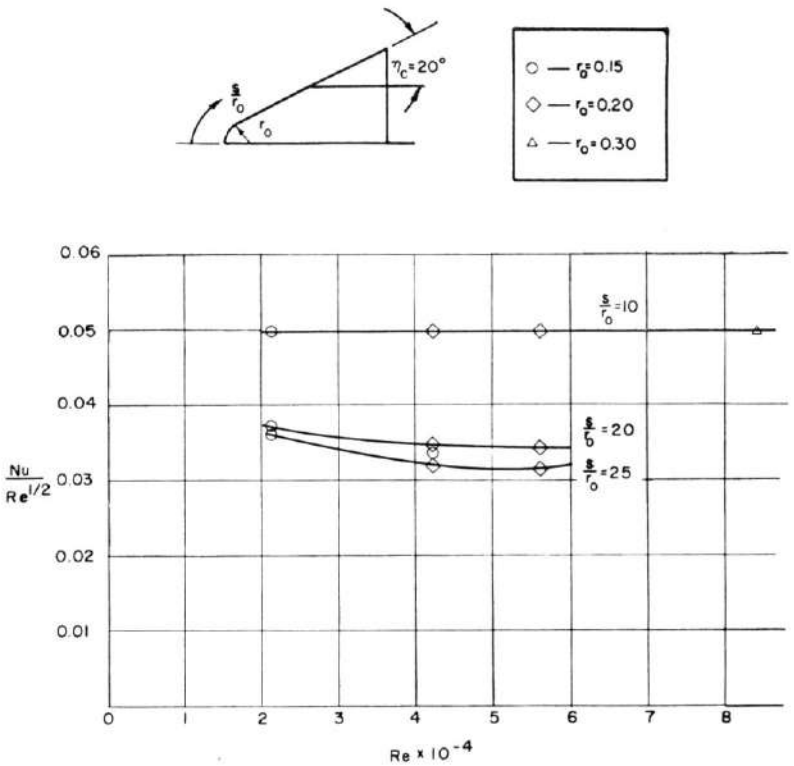

FIG. 32. $Nu/\sqrt{Re}$ at a given station s/r_0 as a function of Re.

Fig. 32 the quantity $Nu/\sqrt{Re}$ is plotted as a function of local Reynolds number for three stations on the body. For the value of $s/r_0 = 10$ the entropy effects are not important because the variation of entropy outside of the boundary layer for the range of variation of the Reynolds number considered is small. For the other two stations this effect starts to be important. In the approximation of conical flow the entropy S outside of the boundary layer is given by

$$S = f\left(B \frac{s}{r_0} \Big/ \sqrt{Re}\right)$$

where $S = f(r/r_0)$ is the relation given by the shape of the shock and B is a constant; therefore S increases and $Nu/\sqrt{Re}$ decreases when $s/r_0\sqrt{Re}$ decreases or for a given s/r_0 when Re increases.

The entropy effects are important in three-dimensional problems. Consider, for example, the elliptical cone of Fig. 17 at $\alpha = 0°$. The mass flow entering the boundary layer in the plane $\Psi = 0°$ crosses the conical shock in the plane $\Psi° = 0$; therefore the entropy outside the boundary layer is constant. However, in the other meridian planes a crossflow component exists and a large entropy gradient exists at the body surface[92]. Because

of this entropy gradient the Nusselt number referred to local conditions at the surface is not proportional to the Reynolds number at the one-half power and is affected by the variation of entropy outside of the boundary layer. In Fig. 17 the $Nu_s/Re_s^{\frac{1}{2}}$ as a function of $s/\sqrt{ab}$ for an elliptical cone at $\alpha=0°$ have been presented for the meridian planes $\Psi=0°$, 35°, 90°. The curves are not straight lines as they would be if the conditions outside the boundary layer were constant as it is usually assumed in boundary layer analyses on cones. The variations for the case of $\alpha=0°$ can be attributed to an entropy effect. The changes of $Nu_s/Re_s^{\frac{1}{2}}$ with $s/\sqrt{ab}$ for $\alpha=0°$ are consistent with the changes expected because of the entropy variations existing outside the boundary layer.

5. CONCLUSIONS

From this brief review of recent developments on hypersonic flow the following conclusions can be made:

(a) The results of theoretical work and of experiments involving simulation of flight conditions tend to indicate that in the approximation within which the physical quantities can be determined and for high flight Reynolds number real gas effects are of relatively small importance.

(b) Pressure distributions and forces on simple boundary conditions can be obtained with simple rough approximations, with accuracy often sufficient for engineering applications. More appreciable progress is required in the development of approximate analyses for more complicated boundary conditions or of more precise analyses for simple problems.

(c) The heat transfer on simple bodies can be obtained with good approximation for the laminar case from existing theories. Simple theories for turbulent cases seem to give sufficient approximation. However, transition phenomena and the foundation of turbulent analysis require much further study.

(d) Entropy gradients can affect heat transfer an appreciable amount and can be utilized to reduce aerodynamic heating at high speed.

LIST OF SYMBOLS

A,B,K coefficients

a,b principal axes of the ellipse

c_p specific heat at constant pressure

D diameter of the body

E internal energy

h enthalpy

h_D average atomic dissociation energy time atom mass fraction in external flow

H height of the cone

k thermal conductivity

L Lewis number for atom, molecule mixture

M Mach number

Nu Nusselt number referred to the nose radius
$Nu = q_w c_{p_s} r_0/k_s (h_{s_e} - h_w)$

Nu_s Nusselt number referred to local position
$Nu = q_w c_{p_s} s/k_s (h_{s_e} - h_w)$

$(Nu)_e$ Nusselt number referred to local external conditions
$Nu = q_w c_{p_e} s/(h_s - h_w) k_e$

P $\log \frac{p}{p_{\text{atm}}}$

Pr Prandtl number $Pr = c_p \mu/k$

p pressure

Q $\log \frac{\rho}{\rho_{\text{atm}}}$

q heat transfer rate B.t.u./ft^2 sec or kW/cm^2

R gas constant

Re Reynolds number referred to the nose radius $Re = \rho_s \sqrt{h_s}\, r_0/\mu_s$.

$\bar{Re}$ modified Reynolds number $\bar{Re} = Re \sqrt{p_s/\rho_s h_s}$

$(Re)_e$ Reynolds number referred to local external conditions
$(Re)_e = \rho_e u_e s/\mu_e$

Re_s Reynolds number referred to local position $\rho_s \sqrt{h_s\, s/\mu_s}$

Re_θ Reynolds number referred to momentum thickness $Re_\theta = \rho_e u_e \theta/\mu_e$

r_0 radius of curvature at the nose

S entropy

s distance along the body surface from the stagnation point

$\tilde{s}$ s/r_0

T temperature

u local velocity

x,y Cartesian co-ordinates

z compressibility factor

Greeks

α angle of attack

γ ratio of specific heat

γ' $= \frac{\rho}{p}\left(\frac{\partial p}{\partial \rho}\right)_s$ Eq. (2.5)

η_c cone half angle

θ angle between the velocity vector and the x-axis, also momentum thickness

μ Mach angle

μ absolute viscosity

ρ density

Ψ co-ordinate of the meridian planes

Subscripts

atm atmospheric conditions at sea-level

e external conditions

L laminar

s stagnation local conditions

s_e stagnation external conditions

t turbulent heat

w wall conditions

0 stagnation free stream conditions

∞ free stream conditions

REFERENCES

1. R. R. GILMORE, Equilibrium Composition and Thermodynamic Properties of Air to 24,000°K, Rand Corporation, RM-1543, 24 August 1955.
2. J. G. LOGAN, Jr., The Calculation of the Thermodynamic Properties of Air at High Temperatures, Cornell Aeronautical Laboratory, Inc., Report No. AD-1052-A-1, AFOSR TN-56-344, May 1956.
3. C. E. TREANOR and J. G. LOGAN, Jr., Thermodynamic Properties of Oxygen from 2000 to 5000°K, Cornell Aeronautical Laboratory, Inc., Report No. BE-1007-A-4, January 1957.
   C. E. TREANOR and J. G. LOGAN, Jr., Thermodynamic Properties of Nitrogen from 2000°K to 8000°K, Cornell Aeronautical Laboratory Inc., Report No. BE-1007-A-5, January 1957.
4. J. HILSENRATH and C. W. BECKETT, Tables of Thermodynamic Properties of Argon-free Air to 15,000°K, Arnold Engineering Development Center AEDC-TN-56-12, September 1956.
5. J. G. LOGAN, Jr. and C. E. TREANOR, Tables of Thermodynamic Properties of Air from 3000 to 10,000°K at Intervals of 100°K, Cornell Aeronautical Laboratory, Inc., Report No. BE-1007-A-3, January 1957.
6. C. FREDERICK HANSEN, Approximations for the Thermodynamic and Transport Properties of High-temperature Air, NACA TN 4150, March 1958.
7. SAUL FELDMAN, Hypersonic Gas Dynamic Charts for Equilibrium Air, AVCO Research Laboratory, January 1957.
8. I. KOROBKIN and S. M. HASTINGS, Mollier Chart for Air in Dissociated Equilibrium at Temperatures of 2000–15,000°K, U.S. Naval Laboratory, NAVORD Report 4446, 23 May, 1957.
9. J. G. LOGAN, Jr., Thermodynamic Charts for High Temperature Air Calculations (2000–9000°K), Cornell Aeronautical Laboratory, Inc., Report No. AD-1052-A-3, AFOSR TN-56-342, July 1956.
10. ADOLF HOCHSTIM, Gas Properties Behind Shocks at Hypersonic Velocities. I. Normal Shocks in Air, Convair Report ZPH (GP)-002, January 1957.
11. S. R. FELDMAN, Hypersonic Conical Shocks for Dissociated Air in Thermodynamic Equilibrium, *Jet Propulsion* Vol. 27, No. 12, p. 1253, December 1957.
12. MARY F. ROMIG, Conical Flow Parameters for Air in Dissociation Equilibrium: Final Results, CONVAIR Research Note 14, January 1958.
13. H. A. BETHE and E. TELLER, Deviations from Thermal Equilibrium in Shock Waves, Ballistic Research Laboratory, Report No. X-117, 1945.
14. GEORGE P. WOOD, Calculations of the Rate of Thermal Dissociation of Air Behind Normal Shock Waves at Mach Numbers of 10, 12 and 14, NACA TN 3634, April 1956.
15. J. G. LOGAN, Jr., Relaxation Phenomena in Hypersonic Aerodynamics, IAS 25th Annual Meeting, Preprint 728, January 1957.
16. N. C. FREEMAN, Dynamics of a Dissociating Gas. III. Non-equilibrium Theory, AGARD Report 133, July 1957.
17. SAUL FELDMAN, The Chemical Kinetics of Air at High Temperatures: A Problem in Hypersonic Aerodynamics, AVCO Research Laboratory, Research Report 4, February 1957. (Also see *J. Fluid Mechanics* Vol. 3, Pt. 3, p. 225, December 1957).
18. V. BLACKMAN, Vibrational Relaxation in Oxygen and Nitrogen. *J. Fluid Mechanics* Vol. 1, Pt. 1, p. 61, May 1956.
19. H. S. GLICK and W. H. WURSTER, Shock Tube Study of Dissociation Relaxation in Oxygen, *J. Chem. Phy.* Vol. 27, No. 5, pp. 1224–1226, November 1957.

20. M. Camac, J. Camm, J. Keck and C. Petty, Relaxation Phenomena in Air Between 3000 and 8000°K, AVCO Research Laboratory, Research Report 22, March 13, 1948.
21. B. Kivel and K. Bailey, Tables of Radiation from High Temperature Air, AVCO Research Laboratory, Research Report 21, December 1957.
22. Steve P. Heims, Effect of Oxygen Recombination on One-dimensional Flow at High Mach Numbers, NACA TN 4144, January 1958.
23. J. A. Fay and F. R. Riddell, Theory of Stagnation Point Heat Transfer in Dissociated Air, *J. Aero. Sci.* Vol. 25, No. 2, pp. 73–85, February 1958.
24. L. Lees, Laminar Heat Transfer Over Blunt-nosed Bodies at Hypersonic Flight Speeds, *Jet Propulsion*, Vol. 26, No. 4, pp. 259–269, April 1956.
25. P. H. Rose and W. I. Stark, Stagnation Point Heat Transfer Measurements in Dissociated Air, *J. Aero. Sci.* Vol. 25, No. 2, pp. 86–97, February 1958.
26. M. Sibulkin, Heat Transfer Near the Forward Stagnation Points of a Body of Revolution, Readers' Forum, *J. Aero. Sci.* Vol. 19, No. 8, pp. 570–571 August 1952.
27. J. V. Becker, Results of Recent Hypersonic and Unsteady Flow Research at the Langley Aeronautical Laboratory, *J. Appl. Phys.* Vol. 21, No. 7, pp. 619–628, July 1950.
28. M. H. Bertram, Viscous and Leading Edge Thickness Effects on the Pressures on the Surface of a Flat Plate in Hypersonic Flow, Readers' Forum, *J. Aero. Sci.* Vol. 21, No. 6, pp. 430–431, June 1954.
29. A. G. Hammitt and S. M. Bogdonoff, A Study of the Flow About Simple Bodies at Mach Numbers from 11 to 15, WADC TR 54-257, October 1954.
30. A. G. Hammitt and S. M. Bogdonoff, Hypersonic Studies of the Leading Edge Effect on the Flow Over a Flat Plate, *Jet Propulsion* Vol. 26, pp. 241–246, April 1956.
31. L. Lees, Influence of the Leading-edge Shock Wave on the Laminar Boundary Layer at Hypersonic Speeds, *J. Aero. Sci.* Vol. 23, No. 6, pp. 594–600, 612, June 1956.
32. F. D. Bennett, Note on Tip-bluntness Effects in the Supersonic and Hypersonic Regimes, Readers' Forum, *J. Aero. Sci.* Vol. 24, No. 4, pp. 314–315, April 1957.
33. A. Ferri and A. Pallone, Note on the Flow Fields on the Rear Part of Blunt Bodies in Hypersonic Flow (Polytechnic Institute of Brooklyn), WADC TN 56-294, July 1956.
34. M. D. Van Dyke, A Model of Supersonic Flow Past Blunt Axisymmetric Bodies with Application to Chester's Solution, *J. Fluid Mechanics* Vol. 3, Pt. 5, pp. 515–522, February 1958.
35. M. J. Lighthill, Dynamics of a Dissociating Gas. Part I. Equilibrium Flow, *J. Fluid Mechanics* Vol. 2, Pt. 1, pp. 1–32, January 1957.
36. Edmund V. Laitone and Otway O'M. Pardee, Location of Detached Shock Wave in Front of a Body Moving at Supersonic Speeds, NACA RM A7B10, 1947.
37. C. C. Lin and S. I. Rubinow, On the Flow Behind Curved Shocks, *J. Math. Phys.* Vol. 27, No. 2, pp. 105–129, July 1948.
38. John Dugundji, An Investigation of the Detached Shock in Front of a Body of Revolution, *J. Aero. Sci.* Vol. 15, No. 12, pp. 699–705, December 1948.
39. Henry T. Nagamatsu, Theoretical Investigation of Detached Shock Waves, Guggenheim Aeronautical Laboratory, California Institute of Technology, GALCIT Publication, 1949.
40. T. Kawamura, On the Detached Shock Wave in Front of a Body Moving at Speeds Greater than that of Sound, *University of Kyoto, College of Science, Memoirs*, Ser. A, Vol. XXVI, No. 3, pp. 207–232, 1950.

41. C. C. LIN and S. F. SHEN, An Analytic Determination of the Flow Behind a Symmetrical Curved Shock in a Uniform Stream, NACA TN 2506, 1951.
42. M. HENRI CABANNES, Contribution à l'étude théorique des fluides compressibles écoulements transsoniques, ondes de choc. Chapitre III. Étude de l'onde de choc détachée au voisinage de son sommet, *Ann. sci. Ec. norm. sup.*, ser. 3, Vol. 69, pp. 31–46.
43. HENRI CABANNES, Détermination théorique de l'écoulement d'un fluide derrière une onde de choc détachée, O.N.E.R.A. Technical Note No. 5, 1951.
44. W. H. HEYBEY, Shock Distances in Front of Symmetrical Bodies, NAVORD Report 3594, 24 December 1953.
45. KINZO HIDA, An Approximate Study on the Detached Shock Wave in Front of a Circular Cylinder and a Sphere, *J. Phys. Soc. Japan* Vol. 8, No. 6, pp. 740–745, November–December 1953. (See also Vol. 10, No. 1, January 1955, pp. 79–81.)
46. H. CABANNES, Tables pour la détermination des ondes de choc détachées *Rech. aéro.*, No. 49, pp. 11–15, January–February 1956.
47. A. BUSEMANN, Flussigkeits und Gasbewegung, 2nd ed., *Handworterbuch der Naturwissenschaften*, pp. 275–277, Gustav Fischer, Jena 1933.
48. H. REESE IVEY, E. BERNARD KLUNKER and N. EDWARD BOWEN, A Method for Determining the Aerodynamic Characteristics of Two- and Three-dimensional Shapes at Hypersonic Speeds, NACA TN 1613, 1948.
49. H. SERBIN, Hypersonic Non-viscous Flow Around a Circular Disk Normal to the Stream, Rand Corporation, RM-1713, 3 May 1956.
50. H. SERBIN, Hypersonic, Non-viscous Flow Around a Sphere, Rand Corporation, RM-1772, 13 August 1956.
51. RONALD F. PROBSTEIN, Inviscid Flow in the Stagnation Point Region of Very Blunt-nosed Bodies at Hypersonic Flight Speeds, Brown University, Division of Engineering, September 1956. (Also published as: WADC TN 56-395, 1956.)
52. W. CHESTER, Supersonic Flow Past a Bluff Body with a Detached Shock. Part I: Two-dimensional Body. Part II: Axisymmetrical Body, *J. Fluid Mechanics*, Vol. 1, Pt. 4, pp. 353–365, October 1956; Vol. 1, Pt. 5, pp. 490–496, November 1956.
53. N. C. FREEMAN, On the Theory of Hypersonic Flow Past Plane and Axially Symmetric Bluff Bodies, *J. Fluid Mechanics*, Vol. 1, Pt. 4, pp. 366–387, October 1956.
54. TING-YI LI and RICHARD E. GEIGER, Stagnation Point of a Blunt Body in Hypersonic Flow, *J. Aero. Sci.* Vol. 24, No. 1, pp. 25–32, January 1957.
55. P. R. GARABEDIAN, Numerical Construction of Detached Shock Waves, *J. Math. Phys.* Vol. 36, No. 3, pp. 192–205, October 1957. (See also: C. C. LIN, Note on Garabedian's Paper "Numerical Construction of Detached Shock Waves", pp. 206–209.)
56. H. M. LIEBERSTEIN and P. R. GARABEDIAN, Examples of Detached Bow Shock Waves in Hypersonic Flow, Paper presented at the 26th Annual Meeting of the Institute of the Aeronautical Sciences, January 1958.
57. MARTIN ZLOTNICK and DONALD J. NEWMAN, Theoretical Calculation of the Flow on Blunt-nosed Axisymmetric Bodies in a Hypersonic Stream, AVCO Manufacturing Company, Report RAD-TR-2-57-29, 19 September 1957.
58. SHIGEO UCHIDA and MICHIRU YASUHARA, The Rotational Field Behind a Curved Shock Wave Calculated by the Method of Flux Analysis, *J. Aero. Sci.* Vol. 23, No. 9, pp. 830–845, September 1956.
59. MILTON VAN DYKE, The Supersonic Blunt-body Problem—Review and Extension, Paper presented at the 26th Annual Meeting of the Institute of the Aeronautical Sciences, January 1958, Preprint No. 801.

60. Roberto Vaglio-Laurin and Antonio Ferri, Theoretical Investigations of the Flow Field About Blunt-nosed Bodies in Supersonic Flight, Gruen Applied Science Laboratories, Inc., Technical Report No. 54, February 1958.

61. K. W. Mangler and M. E. Evans, The Calculation of the Inviscid Flow Between a Detached Bow Wave and a Body, Great Britain, RAE TN Aero. 2536, October 1957.

62. K. G. Guderley, Singularities at the Sonic Velocity, WADC TR 1171-ND, June 1948.

63. S. C. Lin, Cylindrical Shock Waves Produced by Instantaneous Energy Release, *J. Appl. Phys.* Vol. 25, pp. 54–57, January 1954.

64. A. Sakurai, On the Propagation and Structure of the Blast Wave, Part I, *J. Phys. Soc. Japan*, Vol. 8, No. 5, pp. 662–669, September–October 1953; Pt. II, Vol. 9, pp. 256–266, April 1954.

65. L. Lees, Inviscid Hypersonic Flow over Blunt-nosed Slender Bodies. Guggenheim Aeronautical Laboratory, California Institute of Technology, GALCIT Hypersonic Research Project, Memorandum 31, 1 February 1956.

66. H. K. Cheng and A. J. Pallone, Inviscid Leading-edge Effect in Hypersonic Flow, Readers' Forum, *J. Aero. Sci.* Vol. 23, No. 7, pp. 700–702, July 1956.

67. L. Lees and T. Kubota, Inviscid Hypersonic Flow over Blunt-nosed Slender Bodies, *J. Aero. Sci.* Vol. 24, No. 3, pp. 195–202, March 1957.

68. H. R. Ivey, E. G. Klunker and E. N. Bowen, A Method for Determining the Aerodynamic Characteristics of Two- and Three-dimensional Shapes at Hypersonic Speeds, NACA TN 1613, 1948.

69. A. J. Eggers, Jr., R. C. Savin and C. A. Syvertson, The Generalized Shock-expansion Method and its Application to Bodies Travelling at High Supersonic Airspeeds, Paper presented at the Annual Summer Meeting of the Institute of the Aeronautical Sciences, June 1954, Preprint No. 487.

70. V. Halbmillion and C. J. Kulishek, Geometric and Aerodynamic Data on Ogives, U.S. Naval Ordnance Laboratory, NAVORD Report 2239, January 17, 1952.

71. L. Lees, Recent Developments in Hypersonic Flow, *Jet Propulsion* Vol. 27 No. 11, pp. 1162–1178, November 1957.

72. G. Grimminger, E. P. Williams and G. B. W. Young, Lift on Inclined Bodies of Revolution in Hypersonic Flow, *J. Aero. Sci.* Vol. 17, No. 11, pp. 675–690, November 1950.

73. R. M. Machell and W. T. O'Bryant, An Experimental Investigation of Flow Over Blunt-nosed Cones at a Mach Number of 5·8, Guggenheim Aeronautical Laboratory, California Institute of Technology, GALCIT Hypersonic Wind Tunnel Memorandum No. 32, 15 June 1956.

74. W. T. O'Bryant and R. M. Machell, An Experimental Investigation of Flow Over Blunt-nosed Cones at a Mach Number of 5·8, Readers' Forum, *J. Aero. Sci.* Vol. 23, No. 11, pp. 1054–1055, November 1956.

75. Victor Zakkay, Pressure and Laminar Heat Transfer Results in Three-dimensional Hypersonic Flow, Polytechnic Institute of Brooklyn, PIBAL Report No. 447, WADC TN 58-182, September 1958.

76. S. M. Hastings, J. Persh and E. J. Redman, Experimental Investigation of the Pressure Distribution on Axi-symmetric Flat-face Cone-type Bodies at Supersonic and Hypersonic Speeds, NAVORD Report 5659, 1 October 1957.

77. F. W. HARTWIG, Development and Application of a Technique for Steady State Aerodynamic Heat Transfer Measurements, Guggenheim Aeronautical Laboratory, California Institute of Technology, GALCIT Hypersonic Research Project, Memorandum No. 37, 1 June 1957.
78. E. RESHOTKO, Heat Transfer to a General Three-Dimensional Stagnation Point, *Jet Propulsion* Vol. 28, No. 1, pp. 58–59, January 1958.
79. DAVIS H. CRAWFORD and WILLIAM D. MCCAULEY, Investigation of the Laminar Aerodynamic Heat-transfer Characteristics of a Hemisphere-cylinder in the Langley 11-in. Hypersonic Tunnel at a Mach Number of 6·8, NACA Report No. 1323, 1957.
80. R. VAGLIO-LAURIN, Laminar Heat Transfer on Blunt-nosed Bodies in Three-dimensional Hypersonic Flow, Polytechnic Institute of Brooklyn, WADC TN 58-147, May 1958.
81. E. RESHOTKO, Laminar Boundary Layer with Heat Transfer on a Cone at Angle of Attack in a Supersonic Stream, NACA TN 4152, December 1957.
82. PAUL A. LIBBY and ROBERT J. CRESCI, Evaluation of Several Hypersonic Turbulent Heat Transfer Analyses by Comparison with Experimental Data, Polytechnic Institute of Brooklyn, PIBAL Report No. 387, WADC TN 57-72, July 1957.
83. IVAN E. BECKWITH and JAMES J. GALLAGHER, Heat Transfer and Recovery Temperatures on a Sphere with Laminar, Transitional, and Turbulent Boundary Layers at Mach Numbers of 2·00 and 4·15, NACA TN 4125, December 1957.
84. T. E. SHAW, H. S. PERGAMENT and V. DI CRISTINA, General Electric Company, MOSD, Heat Transfer Technical Memorandum 23, June 5, 1956.
85. E. R. VAN DRIEST, The Problem of Aerodynamic Heating, *Aeron. Eng. Rev.* Vol. 15, No. 10, pp. 26–41, October 1956.
86. M. H. BLOOM and A. MARTELLUCCI, A Method for Calculating Turbulent Boundary Layer Properties in High Speed Flow, Gruen Applied Science Laboratories, Inc., Technical Report 27A, March 1957.
87. PAUL A. LIBBY, A Note on the Turbulent Heat Transfer on Blunt-nosed Bodies in Hypersonic Flows (to be published).
88. J. PERSH, A Procedure for Calculating the Boundary Layer Development in the Region of Transition from Laminar to Turbulent Flow, U.S. Naval Ordnance Laboratory, NAVORD Report 4438, March 1957.
89. ANTONIO FERRI and PAUL A. LIBBY, A New Technique for Investigating Heat Transfer and Surface Phenomena Under Hypersonic Flow Conditions, Readers' Forum, *J. Aero. Sci.* Vol. 24, No. 6, pp. 464–465, June 1957.
90. T. Y. LI, Simple Shear Flow Past a Flat Plate in an Incompressible Fluid of Small Viscosity, Readers' Forum, *J. Aeron. Sci.*, Vol. 22, No. 9, pp. 651–652, September 1955.
T. Y. LI, Simple Shear Flow Past a Flat Plate in a Compressible Viscous Field, Readers' Forum, *J. Aero. Sci.* Vol. 22, No. 10, pp. 724–725, October 1955.
T. Y. LI, Effects of Free-stream Vorticity on the Behaviour of a Viscous Boundary Layer, Readers' Forum, *J. Aero. Sci.* Vol. 23, No. 12, pp. 1128–1129, December 1956.
91. M. B. GLAUERT, The Boundary Layer in Simple Shear Flow Past a Flat Plate, Readers' Forum, *J. Aero. Sci.* Vol. 24, No. 11, pp. 848–849, November 1957.
92. RICHARD M. MARK, Effect of Externally Generated Vorticity on Laminar Heat Transfer, Readers' Forum, *J. Aero. Sci.* Vol. 24, No. 12, pp. 923–924, December 1957.
93. ANTONIO FERRI, Supersonic Flow Around Circular Cones at Angles of Attack, NACA Report 1045, 1951.